Premature upregulation of miR-92a's target RBFOX2 hijacks PTBP splicing and impairs cortical neuronal differentiation.

Stephan Weißbach[1,2], Hristo Todorov[2,3], Laura Schlichtholz[2], Sophia Mühlbauer[2], Lea Zografidou[2], Azza Soliman[2], Sarah Lor-Zade[2], Dewi Hartwich[2], Dennis Strand[4], Susanne Strand[4], Tanja Vogel[5], Martin Heine[1], Susanne Gerber[2], Jennifer Winter[2,*]

[1] Institute of Developmental Biology and Neurobiology (iDN), Johannes Gutenberg-University, 55128 Mainz, Germany

[2] Institute of Human Genetics, University Medical Center, Johannes Gutenberg-University, 55131 Mainz, Germany

[3] Current affiliation: Institute of Immunology, University Medical Center, Johannes Gutenberg-University, 55131 Mainz, Germany

[4] Department of Internal Medicine, University Medical Center, Johannes Gutenberg-University, 55131 Mainz, Germany

[5] Institute of Anatomy and Cell Biology, Department of Molecular Embryology, Medical Faculty, Albert-Ludwigs-University Freiburg, 79104 Freiburg, Germany

[*] Corresponding author: jewinter@uni-mainz.de

Abstract

RBFOX2 is an RNA-binding protein crucial for alternative splicing regulation and implicated in several neurodevelopmental disorders. Here, we show that while RBFOX2 is present only at low levels in neural progenitor cells (NPCs), it is upregulated in differentiating neurons of the mouse embryonic neocortex. *In-utero*-electroporation-induced overexpression resulted in a cellular phenotype characterized by impaired neuronal migration and differentiation. Genome-wide analysis at E15.5 revealed numerous alternative splicing events associated with a mixed NPC- and neuron-like splicing pattern and a significant deviation from the normal splicing developmental trajectory. Remarkably, premature *Rbfox2* overexpression induced the inclusion of validated target exons that are otherwise repressed by PTBP2, indicating an antagonistic splicing relationship between these two RNA-binding proteins and highlighting the necessity for strict temporal regulation of their expression during embryonic brain development. Consequently, we showed that the NPC-specific miRNA 92a-3p reduced the expression levels of *Rbfox2 in vitro*. Furthermore, silencing miR-92a-3p *in vivo* in the embryonic neocortex led to a significant increase in *Rbfox2* levels. Our results therefore demonstrate that RBFOX2 is a crucial player in the NPC-to-neuron splicing switch. Furthermore, we present a novel post-transcriptional mechanism for controlling RBFOX2 levels during early neuronal differentiation via miR-92a-3p silencing.

Introduction

Despite the presence of only approximately 22,000 protein-coding genes[1], the murine neocortex, and hippocampus exhibit a considerable diversity of neurons, amounting to 388 transcriptomic cell types, as reported by the Allen Brain Consortium[2]. A key factor enabling this diversity and complexity is alternative splicing (AS), a tightly regulated process that governs the production of multiple mRNA isoforms from a single gene. Intriguingly, nearly every multi-exon gene in the human genome can undergo alternative splicing, generating numerous protein isoforms with distinct structural and

functional properties[3]. This vast molecular diversity expands the proteome's complexity without necessitating a proportional increase in the genome's size. Within the nervous system, AS is a pervasive phenomenon, with various neural genes subject to this regulation[4]. Overall, AS has a higher prevalence across different species and is more conserved in the brain compared to other tissues[5,6].

Specifically, numerous changes in the splicing landscape occur in the developing brain with high temporal precision[4,7]. Among the processes that require correct splicing are neuronal migration, neuronal differentiation[8], axonogenesis[9], and synaptogenesis[10]. Notably, the significance of correct splicing is not confined to the developing brain alone. In the adult brain, different neuronal types exhibit distinct splicing patterns, further underscoring the importance of alternative splicing in maintaining the brain's functional diversity[11,12].

During embryonic development, neural stem cell differentiation requires precise extensive AS switches to create neuron-specific splicing patterns. Many of these splicing events alter key protein domains, particularly in proteins of the cytoskeleton[8]. Various RNA binding proteins (RBPs) regulate the transition from neural stem and progenitor cells to neurons by altering the splicing pattern of target genes, therefore their temporal expression needs to be strictly regulated. Here, microRNAs (miRNAs) that suppress gene expression post-transcriptionally by binding to the 3' untranslated region of target mRNAs[13–16], represent one important mechanism for mediating stage and cell-type specific levels of RBPs For instance, PTBP1 is expressed only in neural stem and progenitor cells, however, it is strongly repressed by miR-124-3p in neurons[17]. In contrast, other prominent RBPs, including NOVA, PTBP2, MBNL2, and RBFOX are predominant in neurons. These RBPs act in both synergistic (e.g. NOVA and RBFOX) and antagonistic relationships (e.g. PTBP1/2 and RBFOX)[18,4,8].

The RBFOX-family consists of three paralogs, namely, RBFOX1 (FOX-1 or A2B1), RBFOX2 (FOX-2 or RBM9) and RBFOX3 (FOX-3, HRNBP3, or NeuN). The association of mutations in human *RBFOX1* and *RBFOX2* with intellectual disability, autism, and other neurodevelopmental disorders, as well as the specific neurological phenotypes observed in *Rbfox* knockout mice, highlight the important functions of these proteins during neurodevelopment[19–26]. All RBFOX-proteins have a single, highly conserved RNA recognition motif (RRM) that binds to the target sequence (U)GCAUG harbored in the premature mRNA and initiates position-dependent splicing. RBFOX binding in the intronic region upstream of an alternatively spliced exon promotes its exclusion from the mature mRNA whereas downstream binding leads to inclusion[27]. Moreover, in humans, all RBFOX-proteins share the position-dependent splicing mechanism and the RRM which is identical in RBFOX1 and RBFOX2 and almost identical in RBFOX3. Therefore, the RBFOX family can act in a functionally redundant manner[28]. However, the temporal expression patterns of these proteins diverge significantly, exhibiting variations across different tissues and cell types[2,11]. In the developing brain, RBFOX proteins are either lowly expressed or not present in neural stem cells, but they are highly expressed in neurons which is in agreement with their role in promoting neuronal differentiation. Studies aiming at identifying splicing changes during neural stem cell differentiation have compared alternative exon usage between NPCs and neurons by RNA-sequencing[8,29]. While these studies have identified numerous splicing changes that are presumably driven by RBFOX binding, the exact role of RBFOX during neuronal differentiation in the embryonic brain has not been elucidated yet.

In the current study, we identified extensive AS changes upon premature *Rbfox2* overexpression in the embryonic neocortex, specifically related to genes that are important for neuronal differentiation and localization. Remarkably, we observed a mixed neuronal and NPC-like splicing pattern that significantly deviated from the normal cortical splicing trajectory. In line with this, *Rbfox2* overexpression increased the percentage of neural stem and progenitor cells and blocked differentiation into neurons on the cellular level. Since a precise and tight control of RBFOX2 is essential for proper neuronal differentiation in the embryonic neocortex, we investigated if miRNAs might repress *Rbfox2* expression in NPCs. Indeed, we observed that the NPC-specific miR-92a led to reduced RBFOX2 levels. Conversely, miR-92a silencing in the embryonic neocortex was associated with a concomitant increase in *Rbfox2* expression.

Results

RBFOX2 is predominantly expressed in neurons

The RBFOX protein family exhibits distinct temporal expression patterns, varying also by cell type. For instance, RBFOX1 and RBFOX3 are expressed in mature neurons and exclusively in the cortical plate in the embryonic cerebral cortex[30] RBFOX2 shows early expression in Purkinje cells in the cerebellum[31]. To elucidate the composition of RBFOX proteins in the mouse embryonic cerebral cortex, we co-stained sections for RBFOX1 and RBFOX2. This confirmed RBFOX2's presence was not limited to the neuron-specific cortical plate, but it was also expressed in the intermediate and ventricular (VZ)/subventricular (SVZ) zones (Figure 1a). In contrast, RBFOX1 expression was restricted to the cortical plate/subplate. While this broader expression pattern of RBFOX2 compared to RBFOX1 was evident, not all cells in the cerebral cortex showed positive RBFOX2 staining. Especially in the VZ/SVZ where radial glia cells and basal progenitors reside at this developmental stage, the majority of cells were RBFOX2 negative (Figure 1a). This prompted us to investigate the temporal expression of RBFOX2 using an *in vitro* neuronal differentiation model. Here, we observed low *Rbfox2* mRNA expression in radial glia-like cells and early neural progenitor cells (NPCs). However, *Rbfox2* expression increased significantly during neuronal differentiation, peaking in late NPCs and young neurons (Figure 1b). Likewise, *Rbfox2* was only weakly expressed in NPCs derived from the embryonic cerebral cortex while it was strongly upregulated in cortical neurons at both RNA and protein levels (Figure 1c, d).

To further corroborate these data, we analyzed RBFOX2 expression in the embryonic cerebral cortex *in vivo* by immunostaining. To this end, we made use of a transgenic mouse model (HES5::GFP) expressing GFP exclusively in Notch-signaling neural progenitor cells. In agreement with the *in vitro* data, RBFOX2 expression was restricted to GFP^{-} cells, that were presumably in a more differentiated state compared to HES5 positive NPCs (Figure 1e). Co-stainings with the basal progenitor marker TBR2 (EOMES) confirmed the absence of RBFOX2 from neural progenitor cells. Only cells with a low TBR2 expression exhibited low RBFOX2 expression, suggesting that these cells were currently differentiating into neurons (Figure 1f). In contrast, RBFOX2 was highly expressed in newborn neurons in all zones as revealed by co-staining with the neuron marker β-III-Tubulin (TUBB3) (Figure 1g). In summary, RBFOX2 was weakly expressed in neural stem and progenitor cells and highly upregulated during neuronal differentiation, highlighting its potential role in mediating the neuron-specific splicing switch.

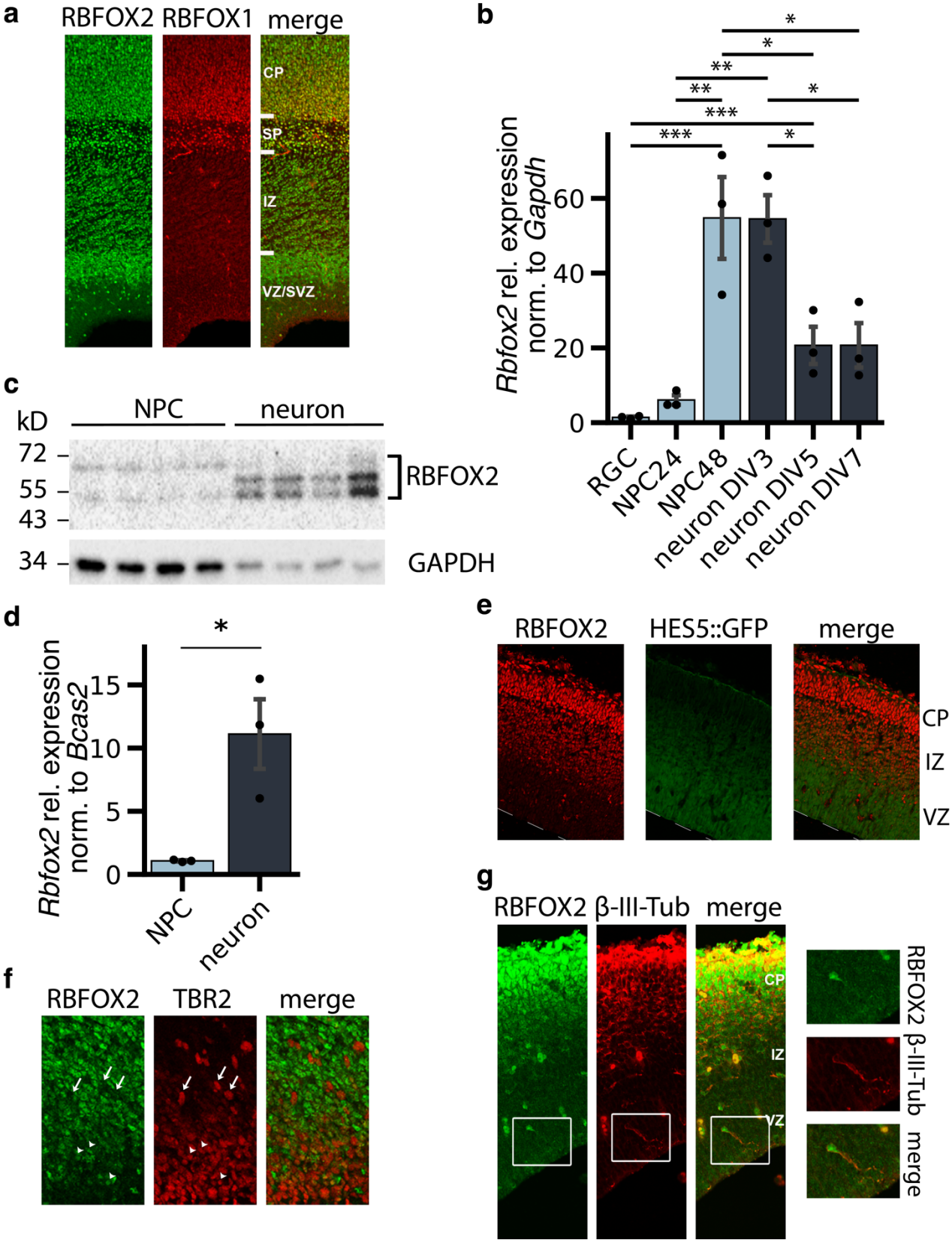

Figure 1 Rbfox2 expression was upregulated in newborn neurons. a) Cryosections of E17.5 cerebral cortex were co-stained with antibodies against RBFOX1 and RBFOX2. Expression of RBFOX1 was restricted to the cortical plate/subplate whereas RBFOX2 was additionally expressed in cells of the ventricular zone (VZ)/subventricular zone (SVZ) and intermediate zone (IZ). b) To determine the expression of Rbfox2 during neuronal differentiation, embryonic stem cells were differentiated into radial glia cells (RGCs), NPCs, and neurons and subjected to RT-qPCR with Rbfox2-specific primers. Rbfox2 expression increased strongly in late NPCs and early neurons and decreased again in late neurons. c) Western blot analysis with RBFOX2-specific antibodies illustrates the increase in RBFOX2 expression in neurons compared to NPCs. Note that due to alternative splicing, several RBFOX2

*isoforms exist which differ between NPCs and neurons. d) RT-qPCR showed increased Rbfox2 expression in neurons compared to NPCs. e) Cryosections of the E14.5 cerebral cortex derived from HES5::GFP transgenic mice were immunostained with RBFOX2 antibodies. RBFOX2 was predominantly expressed in differentiating GFP⁻ cells. f and g) Cryosections of the E17.5 cerebral cortex were co-immunostained for RBFOX2 and the basal progenitor marker TBR2 (f) or RBFOX2 and the newborn-neuron marker β-III-Tubulin (g). RBFOX2 was expressed in β-III-Tubulin+ neurons and absent from TBR2⁺ basal progenitors. *p<0.05, **p<0.01, ***p<0.001, ANOVA followed by Tukey's post-hoc test in b, t-test in d.*

Premature *Rbfox2* overexpression disrupts the splicing landscape of the developing cortex

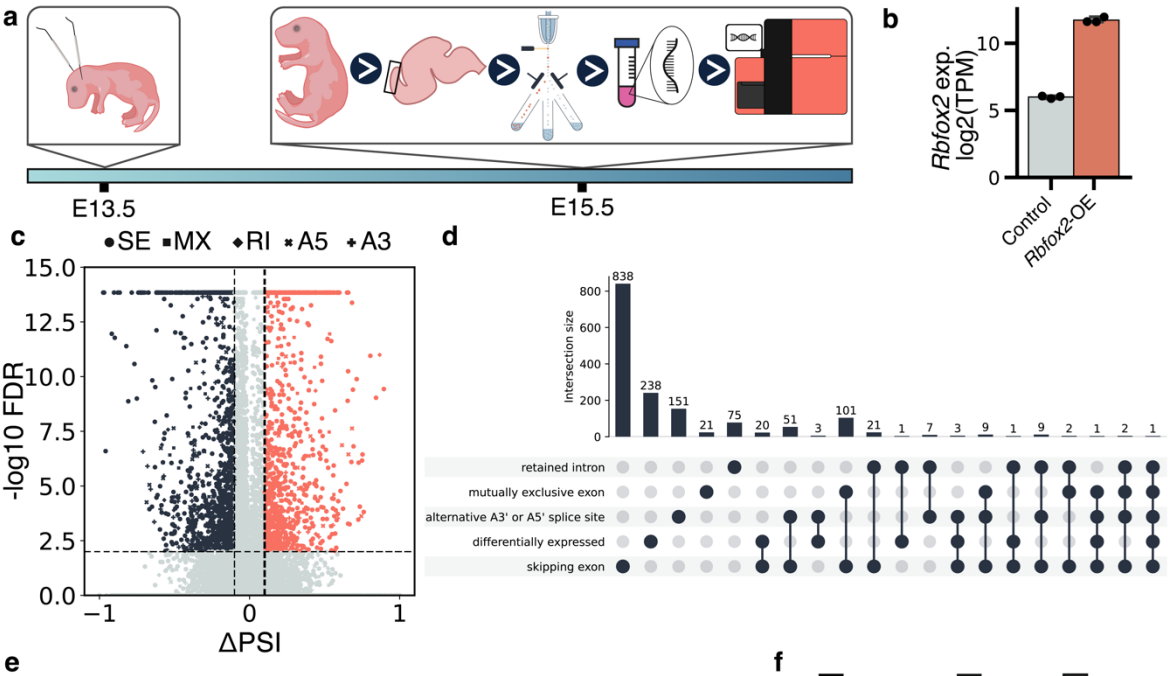

e

Alternative Splicing Event		sig. differentially spliced (FDR < 0.01) ΔPSI > 0.1	ΔPSI < -0.1	Total Events
Skipping Exon		706	877	70,417
Mutually exclusive Exon		112	106	14,750
Retained Intron		29	98	3,565
Alternative 3' Splice Site		38	103	5,314
Alternative 5' Splice Site		46	93	2,150

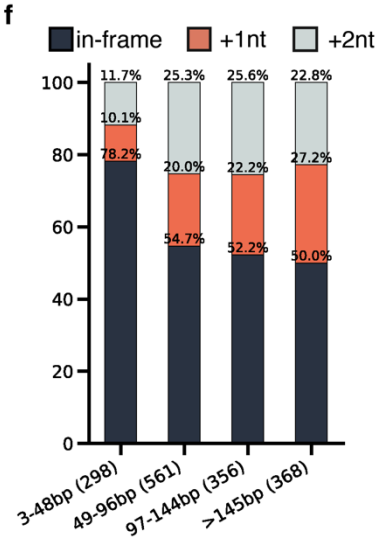

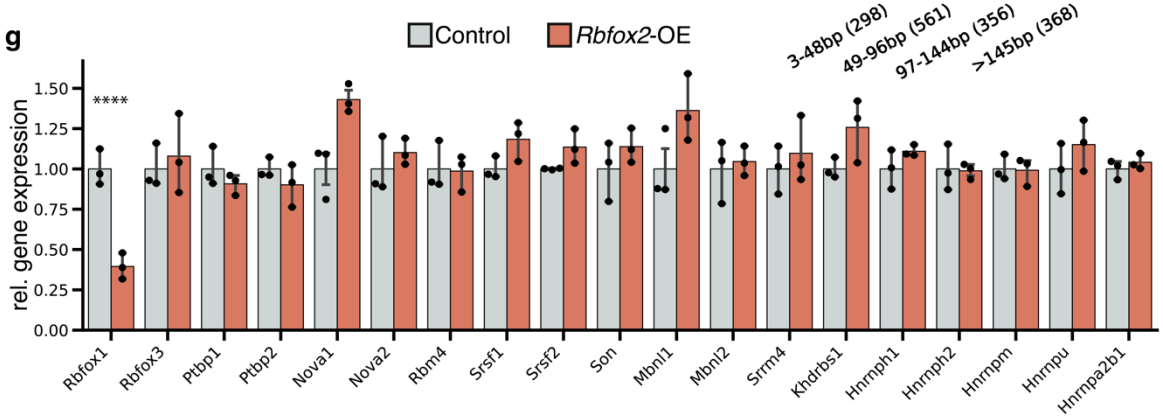

*Figure 2 Rbfox2 overexpression changed the splicing pattern of the developing cortex. a) Experimental timeline, Rbfox2 overexpression was induced in embryonic mouse neocortex at E13.5 by in-utero electroporation, and bulk RNA-sequencing was performed at E15.5 b) The electroporation of Rbfox2 constructs increased the mRNA abundance of Rbfox2 in the cortex significantly c) The volcano plot visualizes alternative splicing events. The x-axis shows delta percentage spliced in (ΔPSI), and the y-axis shows -log10 false discovery rate (FDR) values. Significantly spliced-in events are in orange, spliced-out events are in blue, and non-significant events are in grey. Shapes denote event types: circles for skipping exons, squares for mutually exclusive exons (MX), diamonds for retained introns (RI), and crosses for alternative A5 and A3 splice sites. d) UpSet plot depicts the overlap between 1) Differentially expressed genes, 2) Genes with significant alternatively spliced skipping exon events, 3) Genes with significant alternatively spliced mutually exclusive exon events, and 4) Genes with other splice events, including retained intron, A3', and A5' splice sites. e) The table provides an overview of significant alternative splicing events, totaling 2,208 events. Significance was defined as FDR < 0.01 and either ΔPSI > 0.1 or ΔPSI < -0.1. f) Frequency of induced frameshifts due to alternative splicing for different exon lengths. g) Normalized gene expression levels of key splicing factors important in the CNS, upon Rbfox2 overexpression compared to control. Values for each gene are normalized to the mean of the control group. Data are shown as mean ± standard error of the mean *** p<0.001, ****p<0.0001, Wald test from DESeq2 in g.*

To study RBFOX2's impact on splicing during embryonic corticogenesis, we used *in-utero* electroporation to overexpress *Rbfox2* in the mouse cerebral cortex at E13.5 and subsequently performed RNA-sequencing at E15.5 (Figure 2a). As expected, *in utero* electroporation resulted in a significant increase in *Rbfox2* gene expression (p_{adj} < 0.0001, log2fold = 5.754, Figure 2b). Furthermore, we detected 268 differentially expressed genes (Supplementary Figure S1a, Supplementary Data 1) and substantial changes in the alternative splicing landscape upon *Rbfox2* overexpression (*Rbfox2*-OE) compared to control samples (Figure 2c). However, most alternatively spliced genes did not show altered expression levels. Only 30 genes were alternatively spliced and differentially expressed at the same time (Figure 2d) with *Snhg5*, a lncRNA, having all five types of analyzed splicing events. 17 genes were alternatively spliced and upregulated, while the remaining 13 were downregulated. While frameshifts induced by alternative splicing can result in early stop codons and nonsense-mediated decay (Figure 2f), we did not find significant changes in gene expression related to this phenomenon in our data.

Overall, we detected 2,208 significant alternative splicing events (Figure 2e, Supplementary Figure S2) between the *Rbfox2*-OE and control samples using a stringent threshold of FDR < 0.01 and |ΔPSI| > 0.1. Skipped exons (or cassette exons) represented ~71% of these events. Changes in splicing could mostly be attributed directly to RBFOX2 and not to altered expression of other known splice factors relevant during cortical development (Figure 2g). In line with this, we observed a significant overlap between skipping exon events in our data with *Rbfox* triple knock-out (t*Rbfox*-KO) samples[32] (fold enrichment ≈ 9.833, p-value < 0.0001; Supplementary Figure 3b, Supplementary Data 2). Importantly, inclusion levels of cassette exons present in both data sets were strongly negatively correlated (R = -0.6624, p < 0.0001) indicating that *Rbfox2*-OE induced the opposite splicing regulation compared to t*Rbfox*-KO. (Supplementary Figure 3a). The strong *Rbfox2*-OE induced a significant reduction in the expression level of *Rbfox1* (p_{adj} < 0.0001, log2fold = -1.342). However, the expression of *Rbfox3* was unaltered (p_{adj} ≈ 0.98, log2fold = 0.121) compared to the control group. Remarkably, genes that were alternatively spliced in our analysis were significantly enriched for high-confidence neurodevelopmental disorder (NDD) genes[33] (224 out of 1317 genes, fold enrichment ≈ 1.358, p < 2e-07, Supplementary Data 6, Supplementary Figure S4).

Alternative splicing is a key mediator for the development of proper neuronal functioning. Over 20,000 splicing events have been reported throughout cortical development[34]. To gain a perspective on the splicing pattern induced upon *Rbfox2*-

216 OE, we integrated the previously published RNA-sequencing data from Weyn-
217 Vanhentenryck et al. obtained at different developmental stages of wildtype mouse
218 cerebral cortex (E14.5 to P30)[34] as well as RNA-sequencing from FACS-sorted NPCs
219 and neurons[29]. The hierarchical clustering of splicing events that were significant both
220 in our data and in the previous studies, revealed that our control group clustered with
221 the FACS-sorted neurons as well as with the E14.5 and E16.5 cortical samples. In
222 contrast, the *Rbfox2*-OE group did not closely cluster with any of the embryonic
223 samples or NPCs/neurons pointing to an abnormal splicing pattern (Supplementary
224 Figure S2).
225 To further investigate the impact of *Rbfox2*-OE on the splicing landscape during
226 neurogenesis, we applied a principal component analysis (PCA). We observed a bell-
227 shaped trajectory indicative of the expected splicing changes throughout embryonic
228 and postnatal cortical development (Figure 3a). Remarkably, the influence of batch
229 effects between the different studies was negligible, contrary to differential gene
230 expression analyses where batch effects are often prominent[35,36]. *Rbfox2*-OE resulted
231 in a substantial deviation from this expected developmental trajectory. Specifically, on
232 the first principal component (PC1), *Rbfox2*-OE exhibited a shift towards the splicing
233 pattern associated with mature neurons, while on the second principal component
234 (PC2), the shift was towards undifferentiated NPCs. To identify the main splicing
235 events that explained the observed splicing pattern, we calculated the loadings of the
236 original variables included in the PCA on both PC1 and PC2 (Figure 3b). This analysis
237 revealed numerous genes that are highly relevant for neuronal development.
238 Interestingly, some genes with the highest loadings were associated with
239 neurodevelopmental diseases. For instance, *Shank1* and *Dlgap4* are related to autism
240 spectrum disorder[37,38], whereas *Dlg2* has been linked with schizophrenia[39].
241 To gain insight into the biological processes regulated by the genes that were
242 correlated with each principal component, we performed a gene set enrichment
243 analysis (GSEA) of gene ontology (GO) terms. The loadings of the alternative splicing
244 events on each principal component were used as effect sizes in the GSEA (Figure
245 3c). PC1 was associated with higher-level GO terms such as “regulation of
246 transportation”, “animal organ development”, and “central nervous system
247 development”. This association is plausible given that PC1 represented 55.61% of the
248 variability and separated the samples from early embryonic stage E14.5 to the
249 prepubescent stage P30. During this broad period, manifold biological processes
250 occur, shaping the development of the central nervous system. The higher-level GO
251 terms reflected this complexity as descriptors for the wide-ranging changes captured
252 by PC1. More specifically, transport and localization were significantly enriched for
253 PC1. Interestingly, some splicing events with high PC1 loadings were associated with
254 multiple enriched GO terms. For instance, *Cadps*, a calcium-dependent segregation
255 activator, that was associated with 7 GO terms (Supplementary Data 3), was previously
256 reported to be differentially spliced upon *Rbfox2*-knockout[23]. This gene was also
257 among the top correlated genes of PC1 (Figure 3b, left). Another important gene
258 associated with 6 GO terms was *Ap2a1*. While PTBP2 was previously reported to
259 induce exon skipping in *Ap2a1* (chr7:44,552,885-44,552,951, Supplementary Figure
260 S5a) during brain development[40], *Rbfox2*-OE led to the opposite effect of exon
261 inclusion (FDR < 0.0001, ΔPSI = 0.297) in our data.
262 Moreover, neuron differentiation was among the significant terms associated with PC2,
263 where the *Rbfox2*-OE samples were more similar to an NPC splicing pattern. When
264 analyzing the splicing events that significantly contributed to this GO term, we identified

several developmentally relevant genes. For instance, *Clasp2*, a protein involved in microtubule dynamics, is known to play a role in neuronal migration and axonal growth during cortical development[41]. We detected an alternatively spliced exon in *Clasp2* (chr9:113,691,503-113,691,530, Supplementary Figure S5b) that showed a significantly higher inclusion in the *Rbfox2* overexpression group (FDR < 0.0001, ΔPSI = 0.118). Interestingly, we observed a similar increase of the same exon when analyzing the splicing changes between NPCs and neurons (FDR < 0.01, ΔPSI = 0.118).

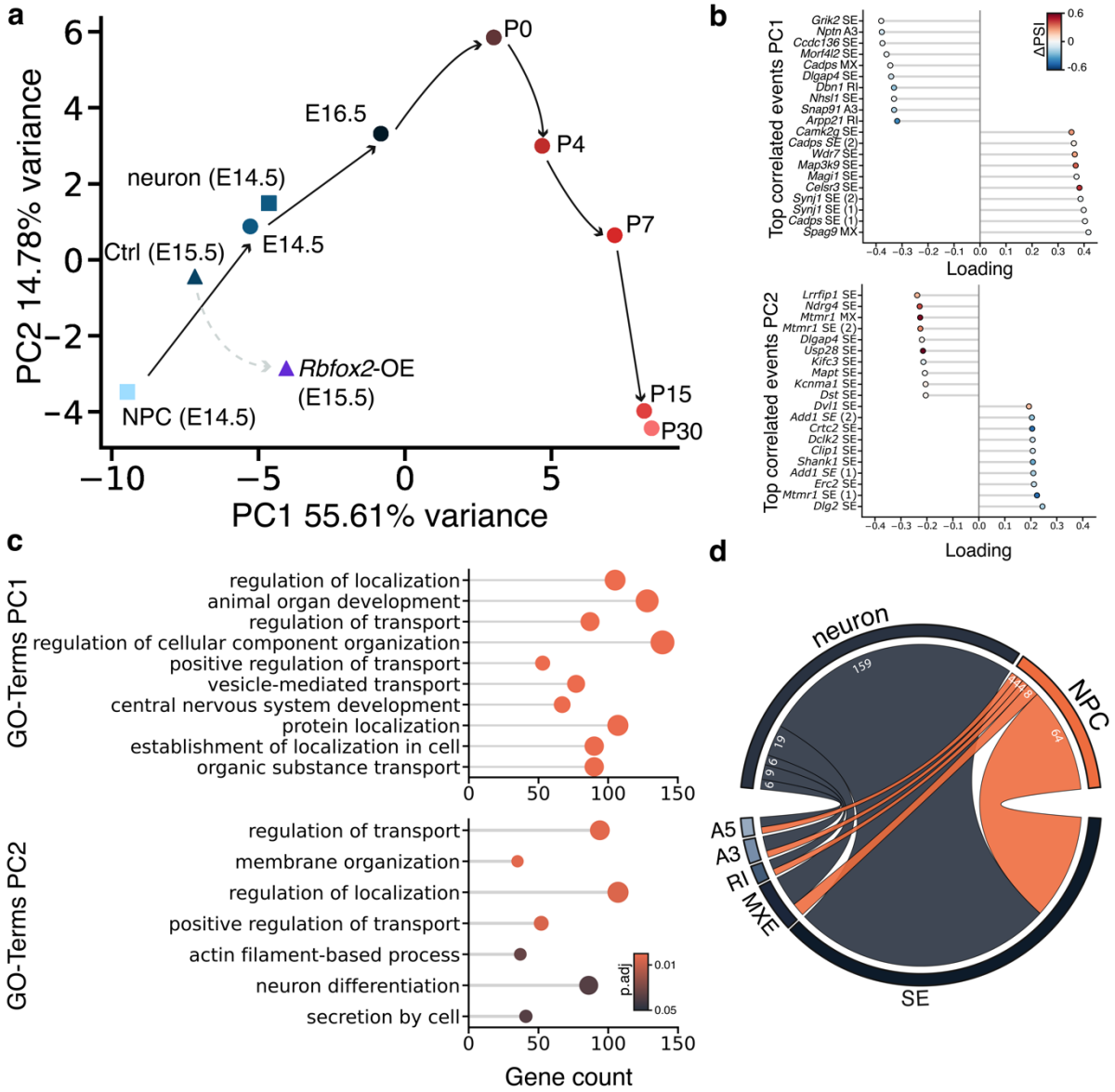

Figure 3 Developmental regulation of alternative splicing by RBFOX2. a) Principal Component Analysis (PCA) of splicing patterns using SplicePCA[42] across embryonic and postnatal brain development. Blue color dots represent embryonic and red dots denote postnatal stages. Shapes indicate the source of the data used. Circles correspond to E14.5 to P30 samples from Weyn-Vanhentenryck et al.[34], squares represent NPC and neuron samples from Liu et al. [43]. Rbfox2 overexpression (OE) samples (triangle shape) noticeably deviate from the expected developmental trajectory. b) Loading analysis for principal component (PC) 1 and PC2, highlighting the top 10 positively and top 10 negatively correlated splicing events for each PC. Color gradient represents the ΔPSI values for Rbfox2-OE compared to control samples c) Gene Set Enrichment Analysis (GSEA) performed on splicing events for PC1 and PC2 using loadings on each component as effect sizes. D) Chord plot showing the association between significant splicing events in Rbfox2-OE vs. control samples compared with splicing events in neurons vs. NPCs obtained using the data from Liu et al. [43].

285 The observed mixed phenotype upon *Rbfox2*-OE was not only characterized by the
286 deviation from the expected developmental trajectory but also by the type of splicing
287 events. When comparing the significant splicing events upon *Rbfox2*-OE with those of
288 neurons vs. NPCs from the Liu et al. data[43], we found an overlap of 283 significant
289 events. Strikingly, 70% of the events corresponded to a neuron-like splicing and 30%
290 of events represent NPC-like splicing patterns (Figure 3d). Several of the overlapping
291 genes have been reported previously to undergo alternative splicing during important
292 developmental processes associated with NPC proliferation, radial migration of
293 neurons, and neuronal differentiation[8]. Genes with a neuron-like splicing included
294 *Clasp2*, *Dctn1*, *Kif2a*, *Mast2*, and *Tpm1*. In contrast, *Add1*, *Clip1*, *Clasp1*, *Dync1i2*,
295 *Gphn*, and *Macf1* were spliced in an NPC-like way (Supplementary Data 4).
296

297 RBFOX2 misexpression impairs neuronal differentiation in the embryonic
298 neocortex

299 After ascertaining the dramatic effect of *Rbfox2* overexpression on the splicing
300 landscape of the developing neocortex, next we investigated whether this translates
301 into changes in neuronal differentiation and/or migration at the cellular level. Therefore,
302 we electroporated *Rbfox2* constructs into the E13.5 neocortex and analyzed brain
303 sections two days later by immunostaining experiments. We detected significantly
304 more RBFOX2-OE cells in VZ and lIZ. Conversely, we observed significantly fewer
305 RBFOX2-overexpressing cells in the uIZ and the CP (Figure 4a). In line with the
306 observed phenotype of cells detaching from the ventricular surface and subsequently
307 failing to migrate to the cortical plate and accumulating in the lIZ, *Rbfox2-OE* induced
308 alternative splicing of two key constituents of the Reelin pathway which plays an
309 important role during cortical development by guiding neurons to the correct position
310 in the CP[44]. Specifically, an exon of *Lrp8* encoding the murine-specific eighth LDL
311 receptor type A (chr4:107,705,477-107,705,600, Supplementary Figure S5f) was
312 abnormally included (FDR < 0.0001, ΔPSI = 0.275). Expression of this exon was
313 previously linked to neuronal migration[45]. Additionally, the exon (chr19:27,217,244-
314 27,217,370, Supplementary Figure S5g) of *Vldlr* encoding the calcium-binding EGF
315 domain was repressed following *Rbfox2*-OE (FDR < 0.0001, ΔPSI = -0.201).
316 Repression of the EGF domain alters the binding affinity to ligands modulating the
317 sensitivity of the receptor and its interacting ligands[46]. Moreover, RBFOX2 could
318 synergistically act with NOVA2 which is known to induce alternative splicing changes
319 in *Dab1*. DAB1 constitutes a switch within the Reelin pathway that is required for
320 neuronal migration[47,48].
321 To investigate the impact of *Rbfox2* misexpression on neuronal differentiation, we
322 performed immunostainings with antibodies against the marker genes PAX6 (radial
323 glia cells), TBR2 (basal progenitors), and SATB2 (neurons). This revealed a significant
324 differentiation defect in the *Rbfox2* overexpressing neocortex. In particular, the
325 percentage of $PAX6^+$ radial glial cells and $TBR2^+$ basal progenitors was significantly
326 increased compared to the control group (Figure 4b,c) whereas the percentage of
327 $SATB2^+$ neurons was reduced (Figure 4d). This indicates that a correct and fine-tuned
328 expression of RBFOX2 is essential for proper neuronal differentiation in the embryonic
329 neocortex.

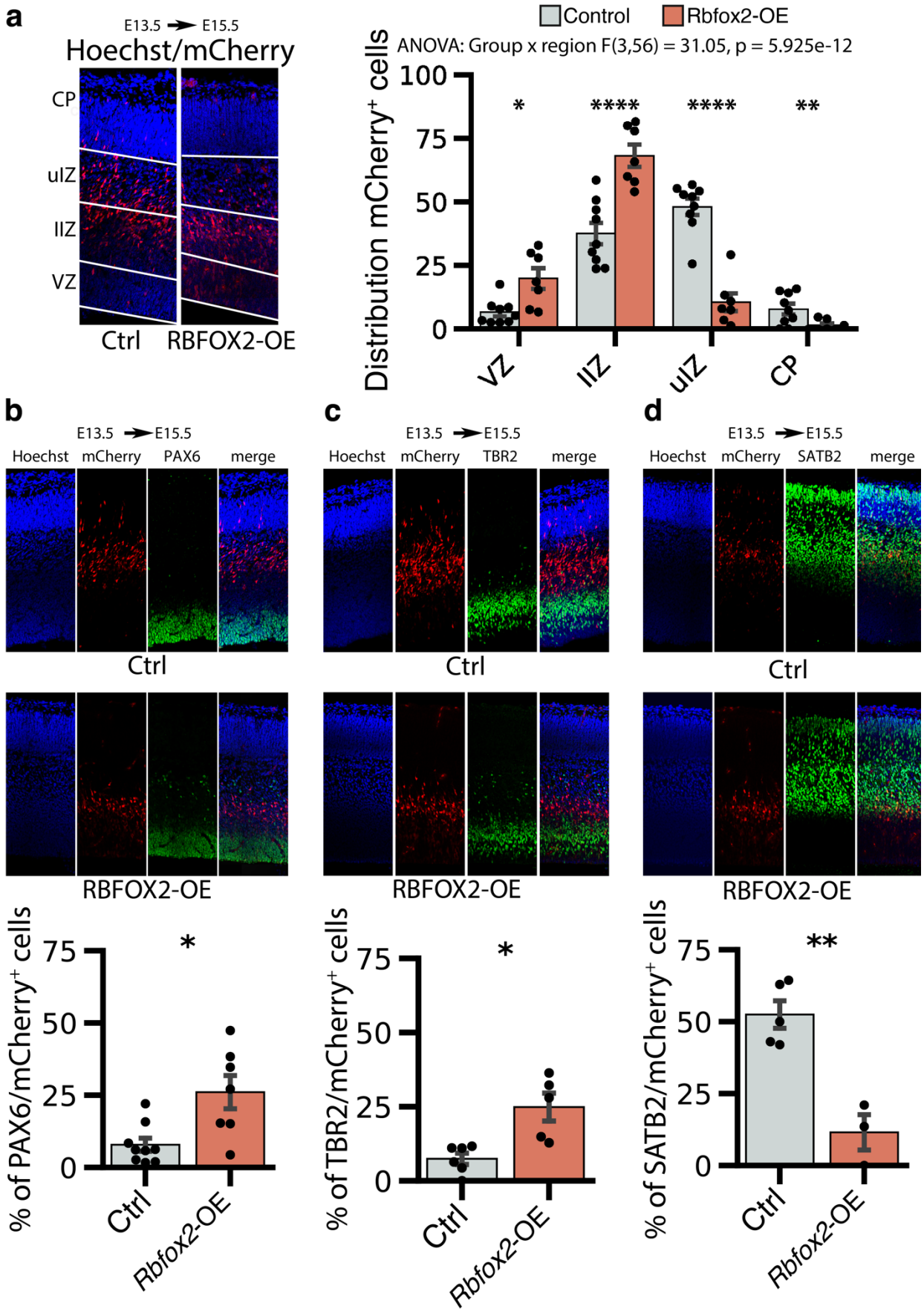

Figure 4 Rbfox2 mis-expression disrupts neuronal differentiation in the neocortex. *Rbfox2 expression constructs were co-electroporated* with *pCAG-mCherry at E13.5. The electroporated brains were analyzed 48 hours later.* a) Distribution of the electroporated mCherry+ cells in the embryonic neocortex. * $p<0.05$, ** $p<0.01$, **** $p<0.0001$, two-way ANOVA followed by pairwise comparison of model means. b-d) Cryosections of the electroporated brains

were immunostained for markers (green) for radial glia cells (b; PAX6), basal progenitors (c; TBR2) and neurons (d; SATB2). Bar plots show mean values ± standard error of the mean. * $p<0.05$, ** $p<0.01$, unpaired t-test in b-d.

RBFOX2 canonical and non-canonical motifs are enriched around alternatively spliced exons

Previous studies have shown that RBFOX1, RBFOX2, and RBFOX3 preferably bind to the conserved sequence (U)GCAUG[49,50]. RBFOX's effect is position-dependent – an upstream intronic binding leads to exon repression, while downstream intronic binding enhances exon inclusion (Figure 5b)[51]. Therefore, we expected to find the canonical motif to be enriched at either location according to the type of alternative splicing events. We screened for all possible pentameric motifs in the 150 nt intronic region directly flanking alternatively spliced cassette exons, accounting for their occurrence in three distinct categories: significantly spliced-in (inclusion), significantly skipped (repression), and unregulated exons (background). To mitigate bias from motifs with higher genome-wide occurrence, we adjusted motif counts of significant splicing events by subtracting background counts and subsequently converted these to z-scores (see Methods).

As expected, the canonical RBFOX motif was enriched downstream of included exons and upstream of repressed exons (Figure 5a). The motif GCAUG was associated with the strongest enrichment, both for upstream binding & exon repression (z-score: 6.8) and downstream binding & exon inclusion (z-score: 9.4). Moreover, shifted motifs such as UGCAU and CAUGC were also enriched and had a high correlation with GCAUG ($r > 0.8$; Supplementary Figure S6). Subsequently, we analyzed the position of the canonical GCAUG for exon inclusion and repression events (Figure 5c). We discovered motifs that promote exon skipping, located both within ~100 nt upstream of the alternatively spliced exon and on the exon itself. Exon inclusion was related to GCAUG occurrence within ~150 nt downstream of the exon. These findings are in line with previous reports on the position-dependent splicing activity of RBFOX2[52,53].

However, we found additional motifs known to be bound by other splicing factors. For instance, UGCUU (z-score 4.9, downstream & exon inclusion) is the preferred motif of muscleblind-like splicing regulator 1 (MBNL1). MBNL1 and RBFOX2 have been found to act synergistically in pluripotent stem cell differentiation[54] and mesenchymal-specific splicing[55]. The relative abundance of MBNL1's motif UGCUU around alternatively spliced exons was only weakly correlated with the abundance of the GCAUG motif ($r=0.27$), therefore both motifs were likely not in close proximity to each other (Supplementary Figure S6).

Surprisingly, we also detected highly enriched poly CU-motifs upstream of included exons, although these are not primary binding sites for RBFOX2. The PTB proteins are known to preferentially bind to these polypyrimidine-rich intronic sequences[56] and to initiate exon exclusion upon binding[57]. Interestingly, these PTBP motifs were enriched upstream of significantly included exons in our data.

To differentiate motifs that are merely abundant around RBFOX2-regulated exons, we analyzed publicly available RBP-RNA interaction data (iClip)[52]. Most of the enriched motifs around alternatively spliced exons upon *Rbfox2*-OE were also confirmed to be bound by RBFOX2 in the iClip data (Figure 5d), specifically the known canonical RBFOX motifs showed high positive z-scores for both data sets. Overall, there was a high correlation between the abundance of motifs around alternatively spliced exons and their presence in iClip peaks (Figure 5e).

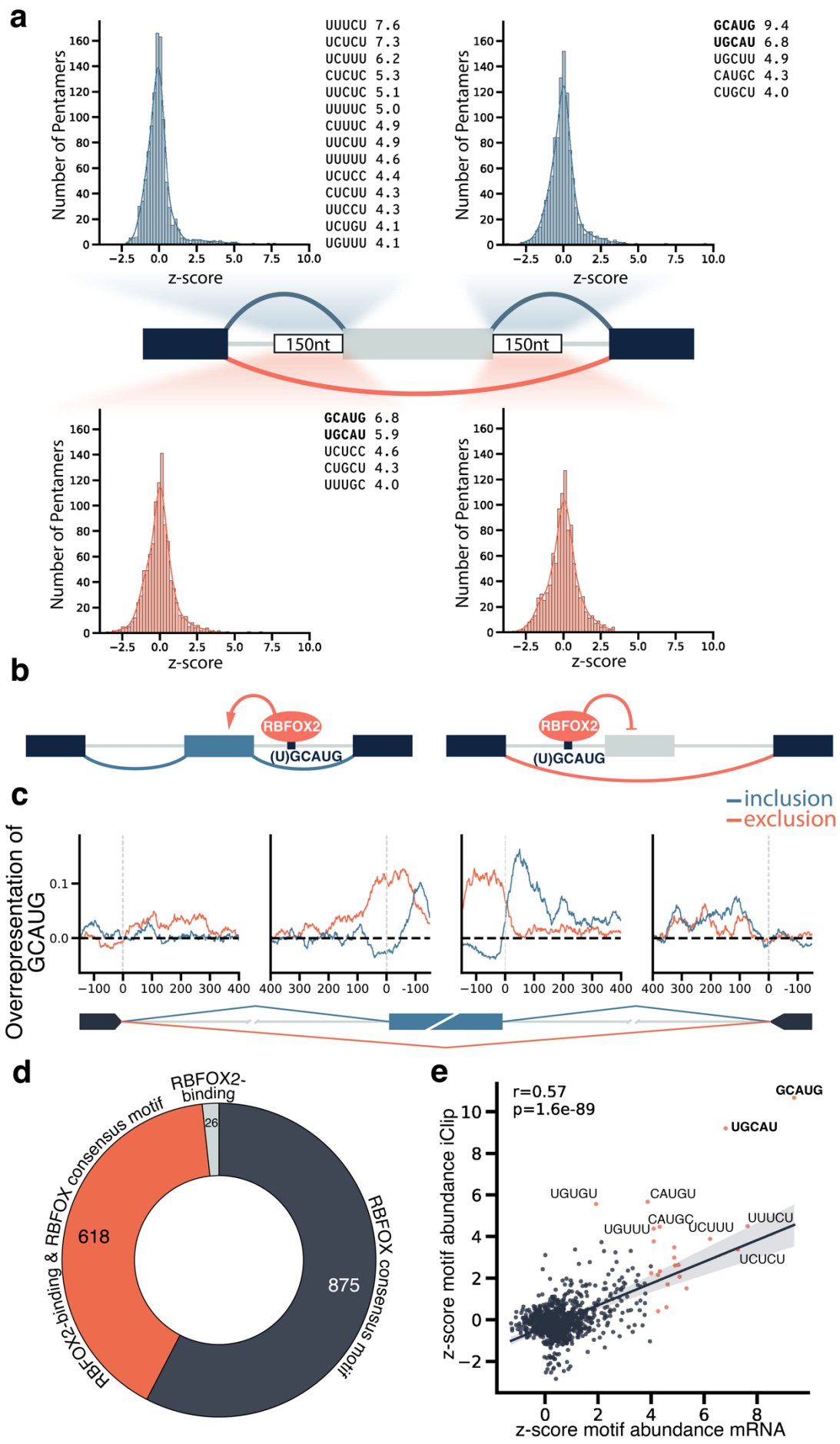
a
Number of Pentamers
z-score
UUUCU 7.6
UCUCU 7.3
UCUUU 6.2
CUCUC 5.3
UUCUC 5.1
UUUUC 5.0
CUUUC 4.9
UUCUU 4.9
UUUUU 4.6
UCUCC 4.4
CUCUU 4.3
UUCCU 4.3
UCUGU 4.1
UGUUU 4.1
GCAUG 9.4
UGCAU 6.8
UGCUU 4.9
CAUGC 4.3
CUGCU 4.0
150nt
150nt
GCAUG 6.8
UGCAU 5.9
UCUCC 4.6
CUGCU 4.3
UUUGC 4.0
b
RBFOX2
(U)GCAUG
RBFOX2
(U)GCAUG
c
inclusion
exclusion
Overrepresentation of GCAUG
d
RBFOX2-binding
26
RBFOX2-binding & RBFOX consensus motif
618
RBFOX consensus motif
875
e
r=0.57
p=1.6e-89
GCAUG
UGCAU
UGUGU
CAUGU
UGUUU
CAUGC
UCUUU
UUUCU
UCUCU
z-score motif abundance iClip
z-score motif abundance mRNA

383

Figure 5 RBFOX2 binding motifs are enriched in the vicinity of alternatively spliced exons. a) Histogram with the frequency of enriched pentameric motifs around alternatively spliced exons in Rbfox2 overexpression (OE) samples versus control. Blue color denotes motifs associated with exon inclusion, while orange represents motifs linked to exon skipping. Known RBFOX2 motifs are indicated with bold font b) Schematic representation of the position-dependent splicing of skipping exons by RBFOX2. c) Relative abundance of the RBFOX2-motif GCAUG in the vicinity of alternatively spliced exons and their flanking exons d) Analysis of alternatively spliced cassette exons reveals that 96% either host an RBFOX motif in the flanking intronic sequence or are bound by RBFOX, as confirmed by iClip data[52]. e) Correlation for position-dependent prevalence of motifs enriched upstream or downstream of alternatively spliced exons in Rbfox2-OE vs. control comparison and in iClip data[52]. Motifs with high correlation are likely recognized by the same splicing factor.

RBFOX2 and PTBP antagonistically shape the transition from NPCs to neurons

The occurrence of the PTBP motifs upstream of significantly spliced-in exons upon *Rbfox2* overexpression hints at antagonistic splicing activities of RBFOX2 and PTBP (Figure 6a). Previous studies have indicated that PTBPs bind to pyrimidine-rich sequences located approximately up to 100 nt upstream of alternatively spliced exons[9,53]. Accordingly, we observed a prominent UCUCU peak in the ~100 nt intronic sequences upstream of exon inclusion events (Figure 6b). Notably, in experiments involving human brain tissue, cell lines, and the mouse cerebral cortex, the upstream occurrence of the PTBP motif was robustly correlated with exon inclusion events. In contrast, in other tissue types, the upstream enrichment of the PTBP motif was associated with exon-skipping[8,53].

These results raise the question of why a potential upstream PTBP binding leads to exon inclusion rather than the expected exclusion in cells of the nervous system.

While previous studies have highlighted an interaction between RBFOX and PTBP1 specifically[8,58–61], the co-regulation of these RBPs may be less relevant in the context of neurodevelopment, as PTBP1 is primarily expressed in non-neuronal cells[17]. We thus hypothesized that simultaneous downstream binding of RBFOX2 might antagonistically overrule the splicing outcome of PTBP and therefore favor exon inclusion. This process could contribute to guiding the transition from immature to mature neuronal splicing. Moreover, PTBP1 and PTBP2 are among the high-confidence protein interaction partners of RBFOX2 (Figure 6c). To investigate whether PTBP and RBFOX2 have antagonistic splicing targets, we first examined all significant cassette exon inclusion events (FDR < 0.01, ΔPSI > 0.1) for the co-occurrence of RBFOX and PTBP motifs. We screened for PTBP-motifs upstream and RBFOX-motifs downstream of alternatively spliced exons and for direct RNA-protein binding sites by reanalyzing iClip data from Vuong et al. for PTBP1 and PTBP2[40] and Jangi et al. for RBFOX2[52]. Roughly 45% of the significant inclusion events (320) had the combination of RBFOX-motif downstream with a PTBP-motif upstream, the majority of these were also highly conserved (Supplementary Figure S7). The cassette exons that were significantly included rarely contained only an RBFOX motif (3) or its binding site (0). The majority of included exons, making up 77.48% (547) of the alternatively spliced exons, harbored either a downstream RBFOX-motif and/or an RBFOX-binding site and simultaneously an upstream PTBP-motif or a PTBP-binding site (Figure 6d).

To corroborate the RBFOX2/PTBP2 antagonistic splicing regulation of cassette exons, we re-analyzed wildtype and *Ptbp2*-KO data of P1 mouse neocortices[40]. We detected 707 alternatively spliced exons in *Ptbp2*-KO (429 included, 187 excluded), with 128 events shared with *Rbfox2*-OE. This represented a 5.241-fold enrichment compared to the expected overlap ($p < 0.0001\%$, Supplementary Figure 8a). Given the proposed antagonistic relationship between both RBPs, we expected *Ptbp2* knockout to induce

435 similar splicing changes as *Rbfox2* overexpression. Indeed, the majority of shared
436 target exons were spliced in the same direction (85.2%, Supplementary Figure 8c).
437 Furthermore, we observed a moderate positive correlation between exon inclusion
438 levels in *Ptbp2*-KO and *Rbfox2*-OE samples ($R = 0.2993$, $p < 0.001$, Supplementary
439 Figure 8b). To further investigate the neurodevelopmental relevance of antagonistic
440 splicing, we analyzed the splicing pattern in our data of 230 PTBP2-repressed exons
441 that were reported to be relevant specifically in the context of neocortical
442 development[40]. *Rbfox2*-OE induced alternative splicing in 67 of these PTBP2 targets.
443 Importantly, the majority of the 67 significant events showed exon inclusion (55) and
444 not exon repression in the *Rbfox2*-OE group (Figure 6e, Supplementary Data 5).
445 Among the antagonistically spliced genes was *Ncam1,* encoding for a cell adhesion
446 protein, that showed an abnormal early exon inclusion (FDR < 0.0001, ΔPSI = 0.148)
447 in the *Rbfox2*-OE condition which led to an increased presence of the exon18
448 (chr9:49,418,152-49,418,953, Supplementary Figure S5c) producing the NCAM-180
449 isoform. Interestingly, the production of alternative isoforms of NCAM occurs during
450 cortical development between E16.5 and P0. In contrast, NCAM140 and NCAM180
451 are the predominant isoforms for neurons, unlike NPCs that express NCAM120 and
452 NCAM140[62].
453 Another PTBP2-excluded[40] and RBFOX2-included cassette exon event was identified
454 in *Kif21b* (chr1:136,101,209-136,101,389, Supplementary Figure S5d). KIF21B is an
455 important regulator of microtubule dynamics. The overexpression of *Rbfox2* induced a
456 highly significant inclusion event (FDR < 0.0001, ΔPSI = 0.305).

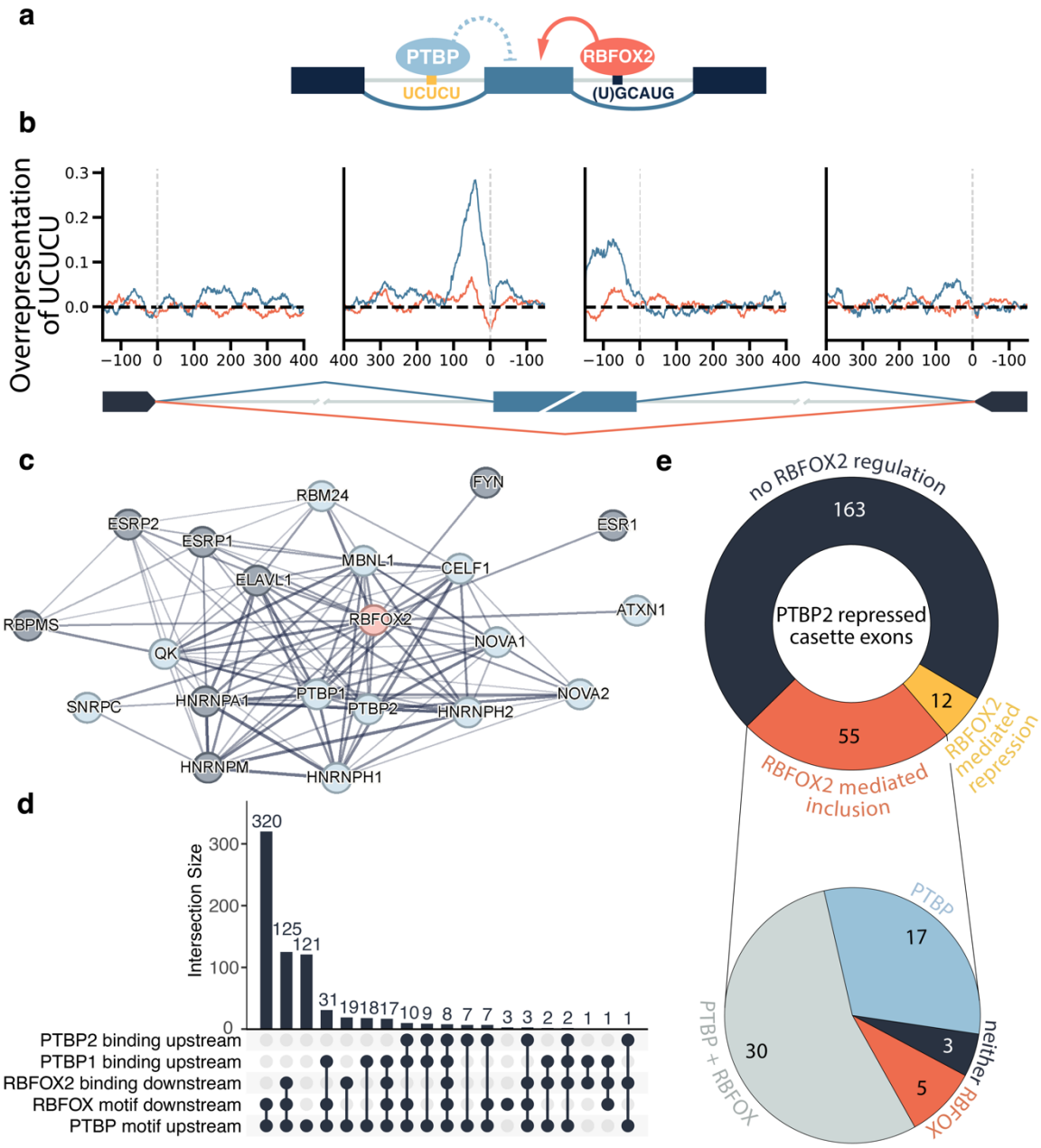

Figure 6 RBFOX and PTBP regulate common targets a) Schematic representation of antagonistic splicing regulation between RBFOX2 and PTBP b) Relative abundance of the PTBP motif UCUCU in the vicinity of alternatively spliced exons in Rbfox2-OE vs. control and their flanking exons. Blue lines indicate exon inclusion and red lines correspond to exon skipping events c) StringDB protein-protein interaction network showing RBFOX2 (orange) and its interaction partners. High-confidence partners are highlighted in light blue d) Bar plot showing the overlap of the presence of RBFOX or PTBP motifs in the flanking intronic sequences of alternatively spliced cassette exons (400 nt) as well as direct RBFOX2 and PTBP2 binding interactions as indicated by the presence of peaks obtained from iClip data[40,52] e) Analysis of developmentally regulated cassette exons suppressed by PTBP2 and the overlap with significantly alternatively spliced exons upon Rbfox2-OE. The donut-shaped circle represents 230 neurodevelopmentally relevant PTBP2-repressed cassette exon events. Colors indicate regulation of these exons upon Rbfox2-OE, blue: unregulated, orange: inclusion, yellow: repression. The lower circle summarizes the presence of conserved binding motifs for RBFOX2 and/or PTBP2 for the exons that are regulated in opposite direction by PTBP2 (repression) and RBFOX2 (inclusion).

Furthermore, exonN (chrX:73,284,421-73,284,478) of the *Flna* transcript was significantly included (FDR < 0.05, ΔPSI = 0.213) upon *Rbfox2*-OE (Supplementary Figure S5e). ExonN was specifically repressed in NPCs and included in neurons (FDR < 0.0001, ΔPSI = 0.4) and the exon inclusion was strongly elevated from E14.5 to E16.5 (FDR < 0.0001, ΔPSI = 0.4205). The iClip[40,52] data also confirmed protein

476 binding for RBFOX2, PTBP1, and PTBP2 in flanking sequences of exonN. *Flna* is an
477 important regulator of neuronal migration[63] and its splicing by PTBP1 in NPCs is
478 associated with shaping the NPC-to-neuron transition during cortical development[8,40].
479 Taken together, our data strongly suggest that RBFOX2 and PTBP have antagonistic
480 roles in controlling alternative splicing, specifically affecting transcripts implicated in
481 neuronal differentiation during cortical development. We identified that a significant
482 portion of alternatively spliced cassette exons are excluded upon PTBP- but included
483 upon RBFOX2-binding in this developmental context.
484

485 miR-92a-3p regulates the expression of *Rbfox2*

486 As we ascertained, NPCs exhibit substantially different splicing patterns compared to
487 neurons (Supplementary Figure S2)[8,43]. Since RBFOX and PTB proteins seemingly
488 regulated antagonistically an overlapping set of developmentally relevant splice
489 targets, we hypothesized that a cell-type, spatially divergent, and time-specific
490 expression of these splice factors would be necessary for normal cortical development.
491 Indeed, *Ptbp1* and *Ptbp2* transcription peaked at E14.5, but contrary to *Ptbp2,* the
492 *Ptbp1* mRNA abundance decreased in the following developmental stages (Figure 7a,
493 right box). Moreover, *Ptbp1* expression is decreased significantly during the transition
494 from NPCs to neurons (Figure 7a, left box) in accordance with previous reports[40,56,64].
495 *Ptbp1* repression is mediated via miR-124-3p, which is a highly specific neuronal
496 miRNA (Figure 7c)[17,65]. Furthermore, miR-124-3p becomes significantly up-regulated
497 in the transition between E14 and E17 of cortical development (Figure 7c)[65].
498 In contrast to *Ptbp1* and *Ptbp2*, *Rbfox2* expression was nearly absent in NPCs and
499 increased significantly in neurons (Figure 1a-b, Figure 7a). In a previous study, we
500 identified 36 miRNAs that were expressed in the embryonic cerebral cortex and
501 predicted to target the 3' untranslated region (3' UTR) of *Rbfox2.* By further inspecting
502 these miRNAs, we observed that most of them were upregulated at E14 followed by a
503 significant reduction of expression levels at the subsequent developmental stages E17
504 and P0 (Supplementary Figure S9)[65]. This prompted us to hypothesize that miRNAs
505 might mediate the low expression levels of *Rbfox2* in NPCs. Specifically, miR-92a-3p
506 was identified as a hub microRNA at E14 during cortical development[65] and it has a
507 predicted binding site in the 3' UTR of *Rbfox2.* Furthermore, the expression of miR-
508 92a-3p was higher in NPCs compared to neurons and decreased gradually from E14
509 to P0 (Figure 7c). Together this data suggests that miRNA-92a-3p might contribute to
510 silencing *Rbfox2* in NPCs at early developmental stages.
511 To follow up on this hypothesis, we performed a luciferase assay using a fragment of
512 the 3' UTR of *Rbfox2* which contained the miR-92a-3p binding site downstream of the
513 *Renilla* luciferase gene. Co-transfection of this reporter plasmid into HEK293 cells
514 together with a miR-92a-3p mimic or a control revealed a reduced luciferase activity of
515 more than two-fold in cells transfected with miR-92a-3p compared to the control. This
516 finding confirmed the gene silencing effect of miR-92a-3p on *Rbfox2* ($p < 0.01$, Figure
517 7d). To investigate the mir-92a-3p-mediated suppression of *Rbfox2 in vivo,* we
518 electroplated mouse embryos at E14.5 with a miR-92a-3p-silencing construct.
519 Expression of miR-92a-3p was reduced more than 10-fold compared to control
520 samples ($p < 0.0001$, Figure 7e). Following miR-92a-3p reduction, we observed a
521 significantly increased *Rbfox2* expression at E16.5 in the miR-92a knock-down
522 samples compared to the control ($p < 0.01$, fold change = 1.571; Figure 7e). To further
523 corroborate these results, we overexpressed miR-92a-3p in an N2A cell culture. This
524 resulted in a significant increase of miR-92a-3p abundance, as measured by RT-qPCR

(p < 0.05, fold change = 2.442; Figure 7f). Importantly, both the mRNA expression (p < 0.05, fold change = 0.748 relative to control; Figure 7f) and the protein levels of RBFOX2 (p < 0.05, fold change = 0.707 relative to control; Figure 7g,h) were reduced significantly upon miR-92a-3p-overexpression.

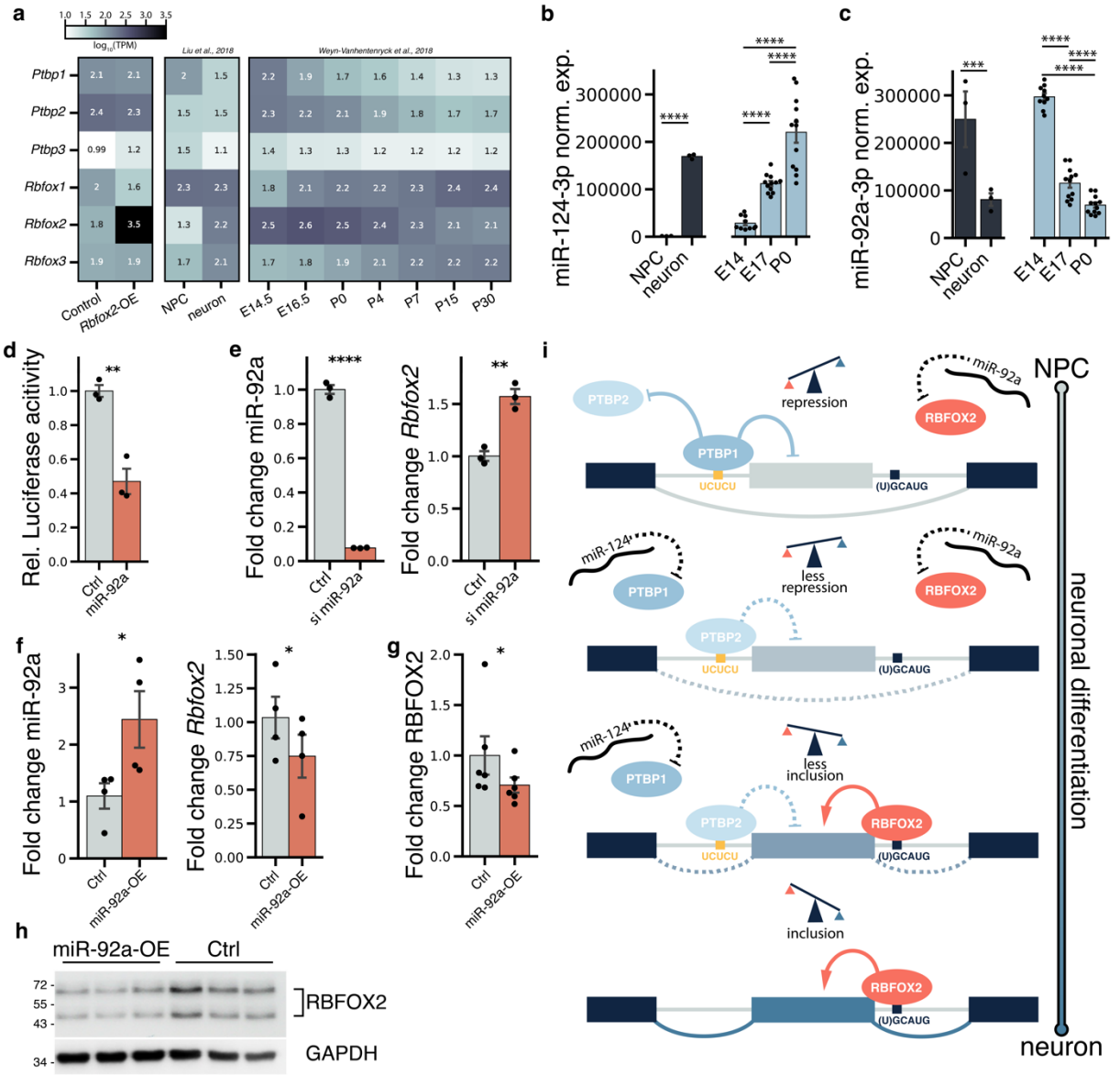

*Figure 7 a) Heatmap showing the gene expression of the RBFOX and PTBP protein families in our study, as well as in NPCs and neurons from Liu et al. [43] and E14.5 to P30 cortical samples obtained from Weyn-Vanhentenryck et al.[34]. Values correspond to log10-transformed transcripts per million (TPM). b) Expression of mir-124-3p known to repress Ptbp1 c) Expression of mir-92a-3p predicted to target Rbfox2. Data on miRNA expression shown in c and d were obtained from Todorov et al.[65] d) Luciferase activity in lysates of HEK293 cells transfected with plasmids containing 3' UTR fragments of Rbfox2 and miR-92a. Fold change of luciferase activity was obtained by calculating the ratio of Renilla luciferase and firefly luciferase activity and then normalizing to the mean of the control. e) In vivo knock-down of miR-92a resulted in a more than 10-fold reduction in miR-92a-3p abundance (left side), and subsequently, Rbfox2 was 1.5-fold enriched (right side). f) Overexpression of miR-92a-3p in N2A cells led to >2-fold enrichment of miR-92a-3p (left side) and subsequently to a decreased abundance of Rbfox2 (right side), as measured by RT-qPCR. h) Overexpression of mir-92a-3p in N2A cells reduced the RBFOX2 protein level significantly. g) Representative image of the western blot for miR-92a overexpression in N2A cells. h) Schematic representation of the proposed splicing mechanism for the transition of immature NPC to mature neurons. Data are shown as mean ± standard error of the mean. *p<0.05, ** p<0.01, *** p<0.001, ****p<0.0001, Wald z-test from DESeq2 in b,c; paired t-test or paired Wilcoxon test in d-g.*

Discussion

RBFOX2 is a crucial component of the complex regulatory network that orchestrates cerebral cortical development. We revealed that misexpression leads to a global disruption of the alternative splicing landscape with a significant overrepresentation of high-confidence NDD risk genes. Consequently, aberrant RBFOX2 splicing activities could produce target gene isoforms that lead to impaired brain development and disorders of the central nervous system in humans[66,67]. For instance, a mutation in *RBFOX2* has been detected previously in a patient with hypoplastic left heart syndrome and NDD[21]. Surprisingly, however, limited research has been conducted on the clinical significance of RBFOX2 as most studies focus on RBFOX1. Mutations in Rbfox1 have been consistently linked with autism spectrum disorder[68–71] and susceptibility to epilepsy[72–74]. Interestingly, *Rbfox1* knock-out resulted in higher seizure susceptibility[75], whereas overexpression was also linked with epilepsy and cortex malformation[76]. Furthermore, reduced cytoplasmic RBFOX1 levels in the prefrontal cortex of individuals with schizophrenia[24] decrease the stability of *Vamp1*, a schizophrenia-associated gene, in PV^+ interneurons[25]. This reduction impairs inhibitory drive from PV^+ interneurons, contributing to schizophrenia pathogenesis[77].

Though RBFOX1 and RBFOX2 have largely overlapping alternative splicing targets[49], the divergent expression patterns we observed here and in previous research indicate that both proteins have common but also distinct functions[23,75,78,79]. To disentangle the specific role of RBFOX2 in the developing brain, we employed an overexpression model instead of a knock-down strategy, as the members of the RBFOX family can compensate for the absence of one of their paralogues[23]. Interestingly, early *Rbfox2*-OE caused a premature detachment and migration of neural cells to the IIZ but not further (Figure 4a). This was accompanied by significant splicing events in key components of the Reelin pathway[44,45] , which plays a crucial role in the migration and localization of cortical neurons and Purkinje cells in the cerebellum. Gehman and colleagues previously showed that the Reelin-binding *Lrp8* gene was alternatively spliced upon *Rbfox2* knock-out. Consequently, Purkinje cells failed to detach and therefore remained near their origin in the VZ[23]. Together with our results, this indicates an important role of RBFOX2 in the initiation and control of cell migration in different parts of the developing nervous system.

Apart from the altered migration, we also observed impaired neuronal differentiation of *Rbfox2*-overexpressing cells (Figure 4b-d). RBFOX2 was specifically upregulated in the transition from NPCs to newly differentiated neurons (Figure 1e), highlighting its role in neural differentiation. Accordingly, we detected a strong alternative splicing pattern in *Numb* which is a key player in asymmetrical neural stem cell division, determining the cell fate of progenitor cells and neurons[80]. Different isoforms of *Numb* can either promote neuronal differentiation or enhance cell proliferation[81], giving a possible explanation for the observed phenotype of decreased neuronal differentiation in our study.

Interestingly, *Rbfox2* expression negatively correlates with expression patterns of the PTBP family. In particular, PTBP1 is a key regulator of non-neuronal splicing in progenitor cells and its repression is required to induce the transition to neurons[17]. In contrast, PTBP2, which is reported to be a weaker repressor of alternatively spliced exons than PTBP1[57,82], is down-regulated by PTBP1 via poison exon inclusion leading to nonsense-mediated decay[17,52,64,83]. Remarkably, our data provided compelling evidence for an antagonistic splicing relationship between RBFOX2 and PTBP.

595 Specifically, RBFOX2 and PTBP2 shared a set of targets that undergo alternative
596 splicing during cerebral cortical development (Figure 6d, e). Although PTBP2 typically
597 promotes the exclusion of these antagonistically spliced exons, RBFOX2 induced the
598 opposite effect of exon inclusion. Therefore, the premature overexpression in our
599 experimental set-up likely led to RBFOX2 overruling the splicing program of PTBP2
600 which could explain the aberrant cellular phenotype and altered splicing landscape we
601 observed. Indeed, several targets that are spliced antagonistically between RBFOX2
602 and PTBP2 play crucial roles, for example, in regulating neuronal differentiation
603 (*Flna*)[8], neurite outgrowth (*Ncam1*), and microtubule dynamics (*Kif21b*). Furthermore,
604 PTBP-recognized motifs are reportedly enriched upstream of alternatively spliced
605 exons that show high inclusion levels in the brain, heart, and skeletal muscles[53]. These
606 tissues are known expression sites of RBFOX2[84] with a concurrent low expression of
607 PTBP1[53]. Therefore, our results and existing reports highlight a complex antagonistic
608 interplay between these proteins in regulating neuronal differentiation[4,8]. Supporting
609 the concept of such dose-sensitive antagonistic interactions among RNA-binding
610 proteins, Ellis and colleagues recently reported that even a modest increase in RBFOX
611 expression levels was sufficient to alter splicing events dependent on another RBP,
612 MBNL1[85]. Furthermore, RBFOX-concentration-dependent splicing regulation has been
613 described in relation to binding to secondary motifs. Accordingly, high RBFOX2 protein
614 levels during neuronal differentiation can mediate exon inclusion through binding to
615 low-affinity motifs[86]. These findings illustrate how nuanced temporal and spatial RBP
616 expression levels enable cell- and developmental-stage specific gene regulation during
617 brain development.
618 Indeed, several post-transcriptional regulatory mechanisms controlling RBFOX levels
619 have been reported already. For instance, sno-lncRNAs can act as sequestering sites
620 for excess RBFOX2 proteins[78]. Furthermore, RBFOX3 can splice poison exons into
621 *Rbfox2* leading to NMD[87]. Another potential layer of regulation is a putative *Rbfox1*-
622 and *Rbfox2*-specific feedback loop. Accordingly, we observed significantly reduced
623 levels of *Rbfox1* following the overexpression of *Rbfox2* (Figure 2g). Similarly, a knock-
624 out of *Rbfox1* was previously reported to lead to an increased level of RBFOX2[75] and
625 vice versa[23]. Furthermore, both RBFOX1 and RBFOX2 contain RBFOX binding sites
626 near a highly conserved 93-nucleotide exon encoding the second half of the RRM.
627 RBFOX binding leads to exon skipping, thereby resulting in a RbfoxΔRRM isoform with
628 significantly reduced RNA binding affinity[88]. In line with this, the *Rbfox2* overexpression
629 in early-stage cortical cells in our study did not result in a complete splicing switch with
630 all regulated exons being either fully spliced in or spliced out.
631 miRNA binding to 3' UTRs represents another key post-transcriptional regulatory
632 mechanism for controlling gene expression and protein levels. In a study investigating
633 the expression patterns of miRNAs in the embryonic cerebral cortex, we recently
634 highlighted targeting of RNA binding proteins as one of the major processes through
635 which miRNAs impact brain development[65]. Similarly to the reported silencing of *Ptbp1*
636 in neurons via miR-124-3p[17], here we showed for the first time that the NPC hub
637 miRNA 92a-3p suppresses the expression of *Rbfox2* (Figure 7f-h). Conversely,
638 silencing miR-92a-3p in the embryonic neocortex led to a significant *Rbfox2*
639 upregulation (Figure 7e, i). In accordance with our results, miR-92a-3p was previously
640 reported to be enriched in intermediate progenitor cells in humans[89,90] and,
641 interestingly, differentially expressed in neurodevelopmental and mental disorders. For
642 instance, levels were elevated in blood[91] and serum[92] of patients with schizophrenia.
643 In contrast, miR-92a-3p was reported to be downregulated in individuals with

644 autism[93,94]. Given the overlapping splicing targets between RBFOX2 and its paralogue
645 RBFOX1, whose mutations have been consistently implicated in such disorders,
646 disruption of the miR-92a-3p/RBFOX2 axis represents an intriguing mechanism for the
647 emergence of diseases of the central nervous system as well as a potential therapeutic
648 target. In particular, future research should focus on elucidating the link between
649 altered miR-92a-3p expression levels and aberrant splicing activities that contribute to
650 disease pathogenesis.
651 Collectively, our results underscore the crucial role of RBFOX2 in the developing
652 cerebral cortex and shed light on the complex interplay with the PTBP family. In our
653 proposed model (Figure 7b), a miRNA-mediated gradual shift from high PTBP levels
654 to a subsequent up-regulation of RBFOX2 shapes neuronal differentiation through a
655 progressive splicing switch from exon exclusion to exon inclusion in commonly
656 regulated targets.
657

658 **Methods**

659 Animals
660 Hes5::GFP mice have been described previously[95]**.** For *in utero* electroporation, timed
661 mated c57BL6/JRj female mice were purchased on gestation day 12 from Janvier
662 (Janvier Labs, Le Genest-Saint-Isle, France), a certified international breeder. Mice
663 were housed in type II long filter top cages (Tecniplast, Buguggiate, Italy) and kept in
664 a 12 h light/dark cycle in a temperature and humidity-controlled animal room (22 ± 2°C,
665 55 ± 5%). Water and food (ssniff M-Z Extrudat, ssniff, Soest, Germany) were supplied
666 *ad libitum*. Mice were treated according to the protocols approved by the local
667 authorities (Landesuntersuchungsamt Rheinland-Pfalz, license number 23 177-07/G
668 13-1-089).
669

670 Constructs
671 HA-tagged full-length *Rbfox2* was cloned into the XhoI and BglII sites of the pCAGGS-
672 mCherry vector using the following primer combinations: *Rbfox2* 1A full-length forward
673 5′-actgctcgaggccaccatgtacccatacgatgttccagattacgctgcggaaggcggccaggcg-3′, with
674 *Rbfox2* reverse 5′-actgagatcttcacgtcacttcagtagg-3′. The miR-92a pre-miRNA
675 including approximately 150 bp of flanking genomic sequence was cloned into the
676 BamHI and EcoRI sites of the pcDNA3.1+ vector using the following primer
677 combinations: miR-92 forward 5′-agtcggatcctttagcgttggaaagtggcc-3′ with miR-92a
678 reverse 5′-agtcgaattctaagttgaggtgtgggtggg-3′. A fragment of the *Rbfox2* 3'UTR
679 containing the miR-92a binding site was cloned into the XbaI site of the pGL3P vector
680 using the following 5'-end phosphorylated oligonucleotides: Sense [Phos] 5′-
681 CTAGACCCCAGTTCATGAGGCCTGGCTATTGCAATATTTACTAGTAGAGGACTC
682 TATAGCT-3′, Antisense [Phos] 5′-CTAGAGCTATAGAGTCCTCTACTAGTAAAT
683 ATTGCAATAGCCAGGCCTCATGAACTGGGGT-3′. Sense and Antisense oligos
684 were annealed in annealing buffer (10mM Tris-HCL; pH 7.5; 0.1 M NaCl; 1 mM EDTA)
685 and cloned into the XbaI site of the pGL3P vector.
686

687 Cell Culture, transfections, and luciferase assays
688 N2A and HEK293 cells were cultured in Dulbecco´s Modified Eagle Medium (DMEM)
689 with 10% fetal bovine serum as well as 1% Penicillin/Streptomycin. For Luciferase
690 assays, HEK293 cells were seeded on 12-well plates at a density of 90,000 cells per
691 well. Twenty-four hours later, the cells were transfected with 400 ng of the constructs

692 cloned into the pGL3P vector, 600 ng miRNA construct and 10 ng pRL-TK vector using
693 the calcium phosphate method. After 48 hours, cells were lysed, and luciferase activity
694 was measured with a CentroXS LB 960 luminometer (Berthold Technologies). N2A
695 cells were transfected with Transfectin reagent (Biorad). The day before the
696 experiment. For transfection, N2A cells were seeded at a density of 250,000 cells per
697 well on 6-well plates. Twenty-four hours later, the cells were transfected with 4000 ng
698 miRNA construct per well. The cells were lysed and processed for RT-qPCR and
699 Westernblot analysis 48 hours after transfection.
700

701 RT-qPCR and Western blot

702 Small RNAs were isolated using the miRNeasy Kit (Qiagen), and total RNA was
703 isolated using the High Pure RNA isolation kit (Roche). TaqMan MicroRNA Assays
704 (Applied Biosystems) were used for miRNA RT-qPCR experiments. The miRNA
705 quantities are relative to U6 snRNA. Total RNA was reverse transcribed using the
706 RevertAid First Strand cDNA Synthesis Kit (Fermentas, Sankt Leon Rot, Germany).
707 For qPCR, SYBR Green Mix was used (TB Green Premix Ex Taq II (RR82WR,
708 Takara)).
709 For Western blot analysis, the cells were lysed, and the proteins were resolved by
710 electrophoresis on SDS acrylamide gels. After transferring the proteins to PVDF
711 membranes, Western blot analyses were performed with antibodies specific for
712 RBFOX2 (rabbit-Anti Rbm9; Bethyl Laboratories) and GAPDH (mouse-Anti GAPDH
713 ab8245, Abcam). Quantification of the bands was performed with ImageJ and
714 normalized to GAPDH band intensity.
715

716 *In utero* Electroporation

717 For *in utero* electroporation, embryonic day E13.5 pregnant female mice were deeply
718 anesthetized with isoflurane, and the uterine horns were exposed. For overexpression,
719 control or *Rbfox2* expression vectors (4 μg/μl) were injected with either pCAG-mCherry
720 or pCAG-eGFP (0.5 μg/μl) into the lateral ventricle of each embryo. For electroporation
721 5 pulses of 40 V for a pulse length of 50 ms at 950-ms intervals were applied
722 (Nepagene, Japan). Subsequently, the uterine horns were returned to the abdominal
723 cavity. After 48 h, the mice were sacrificed by cervical dislocation. The embryos were
724 collected and sacrificed by decapitation. For immunostaining experiments, the brains
725 were isolated, fixed in 4% paraformaldehyde, cryoprotected in 15% and 30% Sucrose
726 solutions, embedded in Cryomatrix (Thermo Scientific), and cryosectioned into 20 μm-
727 thick brain slices.
728 For RNA-sequencing, the brain's GFP^+ area was dissected and digested with trypsin.
729 After stopping the digestion by adding 20% FBS in DMEM and washing with PBS, cells
730 were resuspended in PBS and passed through a 100 μm filter to achieve a single-cell
731 suspension. GFP^+ cells were then collected by fluorescent activated cell sorting
732 (FACS).
733

734 Immunostaining and Imaging

735 For immunostaining, brain cryosections were fixed in 4% paraformaldehyde (PFA) at
736 room temperature (RT) for 10 minutes. After two washes with PBS, antigen retrieval
737 was performed by incubating the slides in 10 mM sodium citrate with 0.5% Tween-20,
738 pH 6, at 80°C for 20 minutes. Subsequently, the sections were blocked in PBS with

739 0.2% Tx-100 containing 2% sheep serum. The sections were then incubated with
740 primary antibody (rabbit anti-RBM9 (Bethyl), mouse anti-RBFOX1 (MABE985,
741 Merck/Millipore, Burlington, MA, USA), rabbit anti-beta III Tubulin (ab18207, Abcam),
742 rabbit Anti-PAX6 (901301, Biolegends), chicken Anti TBR2 (ab34735, Millipore), rabbit
743 Anti-SATB2 (ab34735, Abcam)) in blocking solution overnight at 4°C. The sections
744 were washed three times in PBS 0.2% Tx-100 and incubated in blocking solution
745 containing Alexa-488- or Alexa-594-conjugated secondary antibody (Invitrogen) for 3
746 hours at RT. After three washes in PBS, the sections were embedded in Fluoromount-
747 G with DAPI (00-4959-52, Invitrogen).
748 The sections were viewed using a laser-scanning confocal microscope (LSM710), and
749 images were acquired with the zen software (Zeiss, Oberkochen, Germany). The
750 images were analyzed, and the cells were counted using ImageJ software[96].
751

752 RNA-sequencing

753 NGS library prep was performed with Clontech SMARTer Ultra Low Input RNA Kit for
754 cDNA generation, followed by NuGEN Ovation Ultralow v2 System for library
755 preparation. Libraries were profiled in a DNA 1000 chip on a 2100 Bioanalyzer (Agilent
756 Technologies) and quantified using the Qubit dsDNA HS Assay Kit, in a Qubit 4.0
757 Fluorometer (Invitrogen by Thermo Fisher Scientific). All six samples were pooled in
758 equimolar ratio and sequenced on an Illumina NextSeq 500/550 device.
759

760 RNA-sequencing analysis

761 The paired-end reads were trimmed using BBDuk (version 39.01)[97]. The trimmed
762 reads were mapped to the Gencode reference genome of Mus musculus mm39
763 (released 19.10.2022) using STAR (version 2.7.10b)[98] and the count per gene and
764 sample was determined using FeatureCounts provided by SubRead (version 2.0.6)[99].
765 We used DESeq2 (version 1.40.1)[100] in R (version 4.3.0)[101] to analyze differentially
766 expressed genes with default settings. Since *Rbfox2* was heavily overexpressed, it
767 was removed from the volcano plot for improved visualization. Genes with an adjusted
768 p-value (Benjamini-Hochberg method) < 0.05 were considered to be differentially
769 expressed.
770 rMATS (version 4.1.2)[102] with default settings was used to detect alternatively spliced
771 genes between the *Rbfox2*-OE and control samples. We did not include novel splice
772 events in our analysis. A splicing event with a false discovery rate (FDR) adjusted p-
773 value < 0.01 and an inclusion level difference $|\Delta PSI| > 0.1$ was considered significant.
774 Data processing was done with numpy (version 1.23.5)[103] and pandas (version
775 2.0.1)[104] in Python (version 3.10.12)[105].
776 Plots were generated if not specified otherwise with Matplotlib (version 3.7.1)[106] and
777 seaborn (version 0.12.2)[107].
778 The overlap between significantly alternatively spliced genes and significantly
779 differentially expressed genes was visualized in a five-set Venn diagram with
780 ggVennDiagram (version 1.2.2)[108].
781

782 Analysis of publicly available transcriptomic data sets

783 To further characterize the alternative splicing landscape during cortical development,
784 we re-analyzed two publicly available data sets. The study by Weyn-Vanhentenryck et
785 al. contains RNA-sequencing of the mouse cortex from nine-time points (E14.5, E16.5,
786 P0, P4, P30, 4 months, and 21 months). Sequencing files were downloaded from the

787 NCBI Short Read Archive, accession number SRP055008. The study by Liu et al.
788 contains RNA-sequencing from NPCs and neurons purified from mouse cortices at
789 E15.5, sequencing files were obtained from the Gene Expression Omnibus, accession
790 number GSE96950. Furthermore, we re-analyzed transcriptomic data from *Ptbp2*
791 knockout mouse cortices at P1, obtained from the Gene Expression Omnibus
792 (accession number GSE84803)[40], and triple knockout (*Rbfox*1/2/3) mouse embryonic
793 stem cells, retrieved from the Short Read Archive (accession number SRP128054)[32].
794 The sequencing data were processed according to the protocol specified under the
795 section "RNA-sequencing analysis". The developmental data from Weyn-
796 Vanhentenryck et al. did not allow a pairwise statistical test with rMATS, therefore we
797 conducted a pairwise Fisher's exact test in scipy (version 1.10.1)[109] for consecutive
798 time points and corrected p-values for multiple comparisons by using Benjamini
799 Hochberg's procedure. An event was considered significantly developmentally
800 alternatively spliced when two successive time points had an adjusted p-value < 0.01
801 and $|\Delta PSI| > 0.1$.
802 We used a Monte Carlo simulation to statistically assess the overlap of alternative
803 splicing events (cassette exons) between *Rbfox2*-OE and either t*Rbfox*-KO[32] or *Ptbp2*-
804 KO[40] conditions (see Monte Carlo simulation for details).
805
806 Analysis of publicly available iClip data sets
807 To validate which significant splicing events could be attributable to direct RBFOX2
808 binding, we re-analyzed publicly available iClip data for RBFOX2 expressed in V6.5
809 mESCs. The data was downloaded from NCBI Gene Expression Omnibus, accession
810 number GSE54794[52]. This dataset was supplemented by iClip data for PTBP1 and
811 PTBP2, downloaded from the NCBI short read archive, accession number
812 SRP080878[40].
813 The iClip data was analyzed in several steps. First, we extracted the unique molecular
814 identifiers from the reads using UMI tools (version 1.1.4)[110] and trimmed the adapters
815 with BBDuk (version 39.01)[97]. The trimmed reads were aligned to the reference
816 genome mm39 from Gencode (released 19.10.2022) using STAR (version 2.7.10b)[98].
817 Following the alignment, we removed PCR duplicates by leveraging the unique
818 molecular identifiers with UMI tools. Crosslinking sites were identified as peaks using
819 Clipper[111], which was run within a Docker container based on the image
820 brianyee/clipper:61d5456.
821
822 Inferring the alternative splicing trajectory during cortical development
823 To analyze the effect of *Rbfox2*-overexpression on the alternative splicing pattern
824 concerning normal cortical development, we used the SplicePCA tool[42] integrating our
825 data set with the developmental data of Weyn-Vanhentenryck et al.[4] and Liu et al.[29].
826 We selected events that did not have missing data for any sample and were
827 significantly alternatively spliced in our data and the publicly available data. To
828 investigate how splicing events are correlated with the principal components, we then
829 computed the loading matrix A
830 $$A = V\sqrt{L}$$
831 where V is the matrix of eigenvectors, L is a diagonal matrix with the corresponding
832 eigenvalues and loadings correspond to correlations between the principal
833 components and the original variables[112].
834 For each principal component, we then performed a gene set enrichment analysis
835 (GSEA) using the clusterProfiler package (version 4.8.1)[113,114] in R v4.2.2 with the

biological process ontology, miGSSize of 100, maxGSSize of 500, and an adjusted p-value cut-off of 0.05. The loadings for each gene on the respective principal component were used as input for the GSEA.

Inferring the direction of exon inclusion

To assess whether *Rbfox2*-OE is related to a mature (neuronal) or immature (NPC-specific) splicing pattern, we leveraged the NPC and neuron RNA-sequencing data from Liu et al.[43]. By intersecting our significant alternative splicing results with the Liu et al. data set, we assigned the *Rbfox2*-OE splicing events to three categories: 1) Neuronal direction when the exon inclusion level of the respective gene was significantly higher in neurons than in NPCs in the Liu et al. data; 2) NPC direction when the inclusion level was significantly lower in neurons than in NPC; 3) non-regulated, when the inclusion level was not significantly altered, or the splicing event was not detected in the Liu et al. data set. The results of this analysis were visualized with a chord diagram using the circlize package (version 0.4.15)[115] in R.

Motif enrichment analysis

We performed a *de novo* motif enrichment analysis to identify enriched motifs in the intronic regions located upstream and downstream of alternatively spliced exons. The intronic sequences around alternatively spliced exons (enriched and suppressed exons separately) and a set of background sequences that were not alternatively spliced (FDR > 0.8 and |ΔPSI| < 0.1) were loaded from the mm39 reference genome (Gencode released 19.10.2022) using pysam (version 0.21)[116].
All possible pentameric sequences and their occurrence in the up- and downstream intronic sequences were counted in a sliding window of 50 nt. For each motif, we then subtracted its occurrence in the respective background sequences. Next, motif frequencies were transformed to z-scores using scipy. A motif was considered to be enriched when it had a z-score > 4 ($p < 0.0001$, two-sided z-test).
The iClip peaks were used to validate these predicted motifs. We again screened for the occurrence of every possible pentameric sequence within the peaks of RBFOX2 and the control, subsequently subtracted the respective values, and performed z-scoring. Next, the z-scores of the iClip and RNA-Sequencing motif enrichment analysis were correlated using scipy.

Motif co-occurrence analysis

The co-occurrence of motifs was analyzed similarly to the motif enrichment analysis. 400 nt of intronic sequence flanking the alternatively spliced exon or the exon itself was loaded with pysam (version 0.21.0)[116] and screened for the presence of a PTBP-associated CU-rich motifs (UCUCU, UUUCU, UCUUU, CUCUC, UCUCC, CUCUU, UUCCU)[117] with a z-score > 4 upstream and RBFOX2 canonical motif downstream (GCAUG, UGCAU, CAUGC). Moreover, we integrated confirmed binding sites from the iClip data for RBFOX2[52], PTBP1, and PTBP2[40]. We visualized this using an upset plot[118] and only included overlapping sets with a minimum size of 1.
Further, we examined evolutionarily conserved motif occurrences around these exons by filtering for motifs with a phastcons 35-way[119] score > 0.8.

882 Motif localization map
883 Next, we mapped the localization of the enriched motifs identified in the previous
884 analysis on the alternatively spliced exon and the flanking exons. To the end, we
885 computed the motif density in a sliding window of 50 bp for all up- and downregulated
886 events and background (non-regulated events). Motif density corresponds to the
887 fraction of the 50 nt sliding window that is covered by the motif. The estimates were
888 corrected by subtracting the background density for each motif. This analysis was
889 limited to 150 nt of exonic and 400 nt of intronic sequences spanning up- and
890 downstream from the intron/exon boundaries.
891
892 STRING network analysis
893 Potential interaction partners of RBFOX2 were identified with STRING using all
894 potential interaction sources (version 12.0 beta)[120] allowing 20 interacting proteins and
895 showing confidence as edges. Interactions to RBFOX2 with a confidence score higher
896 than 0.7 were considered high confidence.
897
898 Statistical analysis of immunohistochemistry data
899 Two groups were compared statistically using a t-test or a Wilcoxon test when
900 assumptions of the parametric test were violated, and a data transformation did not
901 improve the model fit. More than two groups were analyzed using one-way or two-way
902 analysis of variance followed by Tukey's post hoc test or post hoc comparison of model
903 means. Data were transformed using a $\log_e$ or an arcsine square root transformation
904 when assumptions of normality and homogeneity of variance were violated. All p-
905 values are two-tailed and a p-value < 0.05 was considered statistically significant.
906 Statistical analysis was performed using R v4.2.2 or Python (version 3.10.12)[105] using
907 scipy (version 1.10.1)[109].
908
909 Overlap of alternatively spliced genes with NDD risk genes
910 Alternatively spliced genes were intersected with high-confidence NDD genes from the
911 GeneTrek database v33[33] to calculate the observed overlap. To obtain a null
912 distribution of the expected overlap, 1317 genes (equal to the total number of
913 alternatively spliced genes upon *Rbfox2*-OE) were randomly sampled from the
914 universe of genes with annotated splice events and the overlap with high-confidence
915 NDD genes and the p-value computed (see Monte Carlo Simulation section for details).
916
917 Monte Carlo Simulation
918 To evaluate the statistical significance of overlaps for various splicing events and
919 genes, Monte Carlo simulations were performed. In each simulation, a number of
920 genes equal to the observed count of alternatively splicing events (t*Rbfox*-KO and
921 *Ptbp2*-KO) or genes (NDD risk genes) were randomly sampled from the universe of
922 genes or splicing events. The overlap with the gene set of interest (e.g., high-
923 confidence NDD genes) was then calculated. This process was repeated 100,000
924 times using a seed of 42 to generate a null distribution of expected overlaps. The p-
925 value was calculated as
926 $$p = 2 * (1 - CDF(zscore))$$
927 using Python (version 3.10.12)[105], numpy (version 1.23.5)[103], and scipy (version
928 1.10.1)[109]. CDF corresponds to the cumulative distribution function of the normal
929 distribution.

Data availability

The RNA Sequencing data generated for this study are available on NCBI SRA (Sequence Read Archive) under the accession number PRJNA1013323.

References

1. Breschi, A., Gingeras, T. R. & Guigó, R. Comparative transcriptomics in human and mouse. *Nat. Rev. Genet.* **18**, 425–440 (2017).
2. Yao, Z. *et al.* A taxonomy of transcriptomic cell types across the isocortex and hippocampal formation. *Cell* **184**, 3222-3241.e26 (2021).
3. Jiang, W. & Chen, L. Alternative splicing: Human disease and quantitative analysis from high-throughput sequencing. *Comput. Struct. Biotechnol. J.* **19**, 183–195 (2021).
4. Weyn-Vanhentenryck, S. M. *et al.* Precise temporal regulation of alternative splicing during neural development. *Nat. Commun.* **9**, 2189 (2018).
5. Raj, B. & Blencowe, B. J. Alternative Splicing in the Mammalian Nervous System: Recent Insights into Mechanisms and Functional Roles. *Neuron* **87**, 14–27 (2015).
6. Barbosa-Morais, N. L. *et al.* The Evolutionary Landscape of Alternative Splicing in Vertebrate Species. *Science* **338**, 1587–1593 (2012).
7. Silbereis, J. C., Pochareddy, S., Zhu, Y., Li, M. & Sestan, N. The Cellular and Molecular Landscapes of the Developing Human Central Nervous System. *Neuron* **89**, 248–268 (2016).
8. Zhang, X. *et al.* Cell-Type-Specific Alternative Splicing Governs Cell Fate in the Developing Cerebral Cortex. *Cell* **166**, 1147-1162.e15 (2016).
9. Zhang, M. *et al.* Axonogenesis Is Coordinated by Neuron-Specific Alternative Splicing Programming and Splicing Regulator PTBP2. *Neuron* **101**, 690-706.e10 (2019).
10. Lin, Y.-S. *et al.* Neuronal Splicing Regulator RBFOX3 (NeuN) Regulates Adult Hippocampal Neurogenesis and Synaptogenesis. *PLOS ONE* (2016).
11. Furlanis, E., Traunmüller, L., Fucile, G. & Scheiffele, P. Landscape of ribosome-engaged transcript isoforms reveals extensive neuronal-cell-class-specific alternative splicing programs. *Nat. Neurosci.* **22**, 1709–1717 (2019).
12. Heck, J. *et al.* More than a pore: How voltage-gated calcium channels act on different levels of neuronal communication regulation. *Channels* **15**, 322–338 (2021).
13. Cai, Y., Yu, X., Hu, S. & Yu, J. A Brief Review on the Mechanisms of miRNA Regulation. *Genomics Proteomics Bioinformatics* **7**, 147–154 (2009).
14. Diederichs, S. & Haber, D. A. Dual Role for Argonautes in MicroRNA Processing and Posttranscriptional Regulation of MicroRNA Expression. *Cell* **131**, 1097–1108 (2007).
15. Lee, R. C., Feinbaum, R. L. & Ambros, V. The C. elegans heterochronic gene lin-4 encodes small RNAs with antisense complementarity to lin-14. *Cell* **75**, 843–854 (1993).
16. Cho, K. H. T., Xu, B., Blenkiron, C. & Fraser, M. Emerging Roles of miRNAs in Brain Development and Perinatal Brain Injury. *Front. Physiol.* **10**, (2019).
17. Makeyev, E. V., Zhang, J., Carrasco, M. A. & Maniatis, T. The MicroRNA miR-124 Promotes Neuronal Differentiation by Triggering Brain-Specific Alternative Pre-

978 mRNA Splicing. *Mol. Cell* **27**, 435–448 (2007).
979 18. Fisher, E. & Feng, J. RNA splicing regulators play critical roles in
980 neurogenesis. *WIREs RNA* **13**, e1728 (2022).
981 19. Bhalla, K. *et al.* The de novo chromosome 16 translocations of two patients
982 with abnormal phenotypes (mental retardation and epilepsy) disrupt the A2BP1 gene.
983 *J. Hum. Genet.* **49**, 308–311 (2004).
984 20. Sebat, J. *et al.* Strong Association of De Novo Copy Number Mutations with
985 Autism. *Science* **316**, 445–449 (2007).
986 21. Homsy, J. *et al.* De novo mutations in congenital heart disease with
987 neurodevelopmental and other congenital anomalies. *Science* **350**, 1262–1266
988 (2015).
989 22. Verma, S. K. *et al.* Rbfox2 function in RNA metabolism is impaired in
990 hypoplastic left heart syndrome patient hearts. *Sci. Rep.* **6**, 30896 (2016).
991 23. Gehman, L. T. *et al.* The splicing regulator Rbfox2 is required for both
992 cerebellar development and mature motor function. *Genes Dev.* **26**, 445–460 (2012).
993 24. O'Leary, A. *et al.* Behavioural and functional evidence revealing the role of
994 RBFOX1 variation in multiple psychiatric disorders and traits. *Mol. Psychiatry* **27**,
995 4464–4473 (2022).
996 25. Vuong, C. K. *et al.* Rbfox1 Regulates Synaptic Transmission through the
997 Inhibitory Neuron-Specific vSNARE Vamp1. *Neuron* **98**, 127-141.e7 (2018).
998 26. Wamsley, B. *et al.* Rbfox1 Mediates Cell-type-Specific Splicing in Cortical
999 Interneurons. *Neuron* **100**, 846-859.e7 (2018).
1000 27. Zhang, C. *et al.* Defining the regulatory network of the tissue-specific splicing
1001 factors Fox-1 and Fox-2. *Genes Dev.* **22**, 2550–2563 (2008).
1002 28. Choi, S. *et al.* Rbfox family proteins make the homo- and hetero-oligomeric
1003 complexes. *Biochem. Biophys. Res. Commun.* **495**, 1022–1027 (2018).
1004 29. Liu, J., Geng, A., Wu, X., Lin, R.-J. & Lu, Q. Alternative RNA Splicing
1005 Associated With Mammalian Neuronal Differentiation. *Cereb. Cortex* **28**, 2810–2816
1006 (2018).
1007 30. Mullen, R. J., Buck, C. R. & Smith, A. M. NeuN, a neuronal specific nuclear
1008 protein in vertebratesxs. *Development* **116**, 201–211 (1992).
1009 31. Gehman, L. T. *et al.* The splicing regulator Rbfox2 is required for both
1010 cerebellar development and mature motor function. *Genes Dev.* **26**, 445–460 (2012).
1011 32. Jacko, M. *et al.* Rbfox Splicing Factors Promote Neuronal Maturation and
1012 Axon Initial Segment Assembly. *Neuron* **97**, 853-868.e6 (2018).
1013 33. Leblond, C. S. *et al.* Operative list of genes associated with autism and
1014 neurodevelopmental disorders based on database review. *Mol. Cell. Neurosci.* **113**,
1015 103623 (2021).
1016 34. Weyn-Vanhentenryck, S. M. *et al.* Precise temporal regulation of alternative
1017 splicing during neural development. *Nat. Commun.* **9**, 2189 (2018).
1018 35. Leek, J. T. *et al.* Tackling the widespread and critical impact of batch effects in
1019 high-throughput data. *Nat. Rev. Genet.* **11**, 733–739 (2010).
1020 36. Weißbach, S. *et al.* Reliability of genomic variants across different next-
1021 generation sequencing platforms and bioinformatic processing pipelines. *BMC*
1022 *Genomics* (2021).
1023 37. Qin, Y. *et al.* A recurrent SHANK1 mutation implicated in autism spectrum
1024 disorder causes autistic-like core behaviors in mice via downregulation of mGluR1-
1025 IP3R1-calcium signaling. *Mol. Psychiatry* **27**, 2985–2998 (2022).
1026 38. Schob, C. *et al.* Cognitive impairment and autistic-like behaviour in SAPAP4-

1027 deficient mice. *Transl. Psychiatry* **9**, 1–19 (2019).
1028 39. Sanders, B. *et al.* Transcriptional programs regulating neuronal differentiation
1029 are disrupted in DLG2 knockout human embryonic stem cells and enriched for
1030 schizophrenia and related disorders risk variants. *Nat. Commun.* **13**, 27 (2022).
1031 40. Vuong, J. K. *et al.* PTBP1 and PTBP2 Serve Both Specific and Redundant
1032 Functions in Neuronal Pre-mRNA Splicing. *Cell Rep.* **17**, 2766–2775 (2016).
1033 41. Dillon, G. M. *et al.* CLASP2 Links Reelin to the Cytoskeleton during
1034 Neocortical Development. *Neuron* **93**, 1344-1358.e5 (2017).
1035 42. Weißbach, S. *et al.* Cortexa – a comprehensive resource for studying gene
1036 expression and alternative splicing in the murine brain. Preprint at
1037 https://doi.org/10.1101/2024.04.11.589045 (2024).
1038 43. Liu, J., Geng, A., Wu, X., Lin, R.-J. & Lu, Q. Alternative RNA Splicing
1039 Associated With Mammalian Neuronal Differentiation. *Cereb. Cortex* **28**, 2810–2816
1040 (2018).
1041 44. Tissir, F. & Goffinet, A. M. Reelin and brain development. *Nat. Rev. Neurosci.*
1042 **4**, 496–505 (2003).
1043 45. Gallo, C. M., Ho, A. & Beffert, U. ApoER2: Functional Tuning Through
1044 Splicing. *Front. Mol. Neurosci.* **13**, (2020).
1045 46. Reddy, S. S., Connor, T. E., Weeber, E. J. & Rebeck, W. Similarities and
1046 differences in structure, expression, and functions of VLDLR and ApoER2. *Mol.*
1047 *Neurodegener.* **6**, 30 (2011).
1048 47. Yano, M., Hayakawa-Yano, Y., Mele, A. & Darnell, R. B. Nova2 Regulates
1049 Neuronal Migration through an RNA Switch in Disabled-1 Signaling. *Neuron* **66**, 848–
1050 858 (2010).
1051 48. Saito, Y. *et al.* Differential NOVA2-Mediated Splicing in Excitatory and
1052 Inhibitory Neurons Regulates Cortical Development and Cerebellar Function: Neuron.
1053 *Neuron* **101**, 707-720.E5 (2019).
1054 49. Weyn-Vanhentenryck, S. M. *et al.* HITS-CLIP and Integrative Modeling Define
1055 the Rbfox Splicing-Regulatory Network Linked to Brain Development and Autism.
1056 *Cell Rep.* **6**, 1139–1152 (2014).
1057 50. Yeo, G. W. *et al.* An RNA code for the FOX2 splicing regulator revealed by
1058 mapping RNA-protein interactions in stem cells. *Nat. Struct. Mol. Biol.* **16**, 130–137
1059 (2009).
1060 51. Zhang, C. *et al.* Defining the regulatory network of the tissue-specific splicing
1061 factors Fox-1 and Fox-2. *Genes Dev.* **22**, 2550–2563 (2008).
1062 52. Jangi, M., Boutz, P. L., Paul, P. & Sharp, P. A. Rbfox2 controls autoregulation
1063 in RNA-binding protein networks. *Genes Dev.* **28**, 637–651 (2014).
1064 53. Castle, J. C. *et al.* Expression of 24,426 human alternative splicing events and
1065 predicted cis regulation in 48 tissues and cell lines. *Nat. Genet.* **40**, 1416–1425
1066 (2008).
1067 54. Venables, J. P. *et al.* MBNL1 and RBFOX2 cooperate to establish a splicing
1068 programme involved in pluripotent stem cell differentiation. *Nat. Commun.* **4**, 2480
1069 (2013).
1070 55. Venables, J. P. *et al.* RBFOX2 Is an Important Regulator of Mesenchymal
1071 Tissue-Specific Splicing in both Normal and Cancer Tissues. *Mol. Cell. Biol.* **33**, 396–
1072 405 (2013).
1073 56. Keppetipola, N., Sharma, S., Li, Q. & Black, D. L. Neuronal regulation of pre-
1074 mRNA splicing by polypyrimidine tract binding proteins, PTBP1 and PTBP2. *Crit.*
1075 *Rev. Biochem. Mol. Biol.* **47**, 360–378 (2012).

1076 57. Ling, J. P. *et al.* PTBP1 and PTBP2 Repress Nonconserved Cryptic Exons.
1077 *Cell Rep.* **17**, 104–113 (2016).
1078 58. Li, Y. I., Sanchez-Pulido, L., Haerty, W. & Ponting, C. P. RBFOX and PTBP1
1079 proteins regulate the alternative splicing of micro-exons in human brain transcripts.
1080 *Genome Res.* **25**, 1–13 (2015).
1081 59. Underwood, J. G., Boutz, P. L., Dougherty, J. D., Stoilov, P. & Black, D. L.
1082 Homologues of the Caenorhabditis elegans Fox-1 Protein Are Neuronal Splicing
1083 Regulators in Mammals. *Mol. Cell. Biol.* **25**, 10005 (2005).
1084 60. Jin, Y. *et al.* A vertebrate RNA-binding protein Fox-1 regulates tissue-specific
1085 splicing via the pentanucleotide GCAUG. *EMBO J.* **22**, 905–912 (2003).
1086 61. Bak, M. *et al.* MAPP unravels frequent co-regulation of splicing and
1087 polyadenylation by RNA-binding proteins and their dysregulation in cancer. *Nat.*
1088 *Commun.* **15**, 4110 (2024).
1089 62. Huang, R. *et al.* NCAM regulates temporal specification of neural progenitor
1090 cells via profilin2 during corticogenesis. *J. Cell Biol.* **219**, e201902164 (2019).
1091 63. Sarkisian, M. R., Bartley, C. M. & Rakic, P. Trouble making the first move:
1092 interpreting arrested neuronal migration in the cerebral cortex. *Trends Neurosci.* **31**,
1093 54–61 (2008).
1094 64. Licatalosi, D. D. *et al.* Ptbp2 represses adult-specific splicing to regulate the
1095 generation of neuronal precursors in the embryonic brain. *Genes Dev.* **26**, 1626–
1096 1642 (2012).
1097 65. Todorov, H. *et al.* Stage-specific expression patterns and co-targeting
1098 relationships among miRNAs in the developing mouse cerebral cortex | bioRxiv.
1099 Preprint at https://doi.org/10.1101/2023.12.16.571081 (2023).
1100 66. Yang, Y. *et al.* Single-cell long-read sequencing in human cerebral organoids
1101 uncovers cell-type-specific and autism-associated exons. *Cell Rep.* **42**, (2023).
1102 67. Chau, K. K. *et al.* Full-length isoform transcriptome of the developing human
1103 brain provides further insights into autism. *Cell Rep.* **36**, (2021).
1104 68. Turner, T. N. *et al.* Genome Sequencing of Autism-Affected Families Reveals
1105 Disruption of Putative Noncoding Regulatory DNA. *Am. J. Hum. Genet.* **98**, 58–74
1106 (2016).
1107 69. Bacchelli, E. *et al.* An integrated analysis of rare CNV and exome variation in
1108 Autism Spectrum Disorder using the Infinium PsychArray. *Sci. Rep.* **10**, 3198 (2020).
1109 70. Griswold, A. J. *et al.* Targeted massively parallel sequencing of autism
1110 spectrum disorder-associated genes in a case control cohort reveals rare loss-of-
1111 function risk variants. *Mol. Autism* **6**, 43 (2015).
1112 71. Kanduri, C. *et al.* The landscape of copy number variations in Finnish families
1113 with autism spectrum disorders. *Autism Res.* **9**, 9–16 (2016).
1114 72. Fanciulli, M. *et al.* Copy number variations and susceptibility to lateral temporal
1115 epilepsy: A study of 21 pedigrees. *Epilepsia* **55**, 1651–1658 (2014).
1116 73. Lal, D. *et al.* Rare exonic deletions of the RBFOX1 gene increase risk of
1117 idiopathic generalized epilepsy. *Epilepsia* **54**, 265–271 (2013).
1118 74. Lal, D. *et al.* Extending the phenotypic spectrum of RBFOX1 deletions:
1119 Sporadic focal epilepsy. *Epilepsia* **56**, e129–e133 (2015).
1120 75. Gehman, L. T. *et al.* The splicing regulator Rbfox1 (A2BP1) controls neuronal
1121 excitation in the mammalian brain. *Nat. Genet.* **43**, 706–711 (2011).
1122 76. Wen, M. *et al.* Upregulation of RBFOX1 in the malformed cortex of patients
1123 with intractable epilepsy and in cultured rat neurons. *Int. J. Mol. Med.* **35**, 597–606
1124 (2015).

1125 77. Chung, Y. *et al.* Altered Rbfox1-Vamp1 pathway and prefrontal cortical
1126 dysfunction in schizophrenia. *Mol. Psychiatry* 1–10 (2024) doi:10.1038/s41380-024-
1127 02417-8.
1128 78. Conboy, J. G. Developmental regulation of RNA processing by Rbfox proteins.
1129 *WIREs RNA* **8**, e1398 (2017).
1130 79. Mukherjee, A. & Nongthomba, U. To RNA-binding and beyond: Emerging
1131 facets of the role of Rbfox proteins in development and disease. *WIREs RNA* **15**,
1132 e1813 (2023).
1133 80. Cayouette, M. & Raff, M. Asymmetric segregation of Numb: a mechanism for
1134 neural specification from Drosophila to mammals. *Nat. Neurosci.* **5**, 1265–1269
1135 (2002).
1136 81. Gulino, A., Di Marcotullio, L. & Screpanti, I. The multiple functions of Numb.
1137 *Exp. Cell Res.* **316**, 900–906 (2010).
1138 82. Keppetipola, N. M. *et al.* Multiple determinants of splicing repression activity in
1139 the polypyrimidine tract binding proteins, PTBP1 and PTBP2. *RNA* **22**, 1172–1180
1140 (2016).
1141 83. Linares, A. J. *et al.* The splicing regulator PTBP1 controls the activity of the
1142 transcription factor Pbx1 during neuronal differentiation. *eLife* **4**, e09268 (2015).
1143 84. Uhlén, M. *et al.* Tissue-based map of the human proteome. *Science* **347**,
1144 1260419 (2015).
1145 85. Ellis, J. A., Hale, M. A., Cleary, J. D., Wang, E. T. & Andrew Berglund, J.
1146 Alternative Splicing Outcomes Across an RNA-Binding Protein Concentration
1147 Gradient. *J. Mol. Biol.* **435**, 168156 (2023).
1148 86. Begg, B. E., Jens, M., Wang, P. Y., Minor, C. M. & Burge, C. B. Concentration-
1149 dependent splicing is enabled by Rbfox motifs of intermediate affinity. *Nat. Struct.*
1150 *Mol. Biol.* **27**, 901–912 (2020).
1151 87. Dredge, B. K. & Jensen, K. B. NeuN/Rbfox3 Nuclear and Cytoplasmic
1152 Isoforms Differentially Regulate Alternative Splicing and Nonsense-Mediated Decay
1153 of Rbfox2. *PLOS ONE* **6**, e21585 (2011).
1154 88. Damianov, A. & Black, D. L. Autoregulation of Fox protein expression to
1155 produce dominant negative splicing factors. *RNA* **16**, 405–416 (2010).
1156 89. Nowakowski, T. J. *et al.* Regulation of cell-type-specific transcriptomes by
1157 microRNA networks during human brain development. *Nat. Neurosci.* **21**, 1784–1792
1158 (2018).
1159 90. Florio, M. *et al.* Human-specific gene ARHGAP11B promotes basal progenitor
1160 amplification and neocortex expansion. *Science* **347**, 1465–1470 (2015).
1161 91. Ma, J. *et al.* Identification of miR-22-3p, miR-92a-3p, and miR-137 in
1162 peripheral blood as biomarker for schizophrenia. *Psychiatry Res.* **265**, 70–76 (2018).
1163 92. Shi, W. *et al.* Aberrant expression of serum miRNAs in schizophrenia. *J.*
1164 *Psychiatr. Res.* **46**, 198–204 (2012).
1165 93. Talebizadeh, Z., Butler, M. G. & Theodoro, M. F. Feasibility and relevance of
1166 examining lymphoblastoid cell lines to study role of microRNAs in autism. *Autism*
1167 *Res.* **1**, 240–250 (2008).
1168 94. Huang, F. *et al.* Investigation of Gene Regulatory Networks Associated with
1169 Autism Spectrum Disorder Based on MiRNA Expression in China. *PLOS ONE* **10**,
1170 e0129052 (2015).
1171 95. Basak, O. & Taylor, V. Identification of self-replicating multipotent progenitors
1172 in the embryonic nervous system by high Notch activity and Hes5 expression. *Eur. J.*
1173 *Neurosci.* **25**, 1006–1022 (2007).

1174 96. Schindelin, J. *et al.* Fiji: an open-source platform for biological-image analysis.
1175 *Nat. Methods* **9**, 676–682 (2012).
1176 97. BBMap. *SourceForge* https://sourceforge.net/projects/bbmap/ (2022).
1177 98. Dobin, A. *et al.* STAR: ultrafast universal RNA-seq aligner. *Bioinformatics* **29**,
1178 15–21 (2013).
1179 99. Liao, Y., Smyth, G. K. & Shi, W. featureCounts: an efficient general purpose
1180 program for assigning sequence reads to genomic features. *Bioinformatics* **30**, 923–
1181 930 (2014).
1182 100. Love, M. I., Huber, W. & Anders, S. Moderated estimation of fold change and
1183 dispersion for RNA-seq data with DESeq2. *Genome Biol.* **15**, 550 (2014).
1184 101. R Core Team. R: A language and environment for statistical computing. R
1185 Foundation for Statistical Computing (2022).
1186 102. rMATS: Robust and flexible detection of differential alternative splicing from
1187 replicate RNA-Seq data | PNAS.
1188 https://www.pnas.org/doi/10.1073/pnas.1419161111.
1189 103. Array programming with NumPy | Nature.
1190 https://www.nature.com/articles/s41586-020-2649-2.
1191 104. team, T. pandas development. pandas-dev/pandas: Pandas. Zenodo
1192 https://doi.org/10.5281/zenodo.8092754 (2023).
1193 105. The Python Language Reference — Python 3.10.12 documentation.
1194 https://docs.python.org/3.10/reference/.
1195 106. Matplotlib: A 2D Graphics Environment | IEEE Journals & Magazine | IEEE
1196 Xplore. https://ieeexplore.ieee.org/document/4160265.
1197 107. Waskom, M. L. seaborn: statistical data visualization. *J. Open Source Softw.* **6**,
1198 3021 (2021).
1199 108. Gao, C.-H., Yu, G. & Cai, P. ggVennDiagram: An Intuitive, Easy-to-Use, and
1200 Highly Customizable R Package to Generate Venn Diagram. *Front. Genet.* **12**,
1201 (2021).
1202 109. Virtanen, P. *et al.* SciPy 1.0: fundamental algorithms for scientific computing in
1203 Python. *Nat. Methods* **17**, 261–272 (2020).
1204 110. Smith, T., Heger, A. & Sudbery, I. UMI-tools: modeling sequencing errors in
1205 Unique Molecular Identifiers to improve quantification accuracy. *Genome Res.* **27**,
1206 491–499 (2017).
1207 111. Lovci, M. T. *et al.* Rbfox proteins regulate alternative mRNA splicing through
1208 evolutionarily conserved RNA bridges. *Nat. Struct. Mol. Biol.* **20**, 1434–1442 (2013).
1209 112. Todorov, H., Fournier, D. & Gerber, S. Principal components analysis: theory
1210 and application to gene expression data analysis. *Genomics Comput. Biol.* **4**, 100041
1211 (2018).
1212 113. Wu, T. *et al.* clusterProfiler 4.0: A universal enrichment tool for interpreting
1213 omics data. *The Innovation* **2**, 100141 (2021).
1214 114. Yu, Guangchuang, Wang, Li-Gen, & He, Qing-Yu. clusterProfiler: an R
1215 Package for Comparing Biological Themes Among Gene Clusters. *OMICS J. Integr.*
1216 *Biol.* **16**, 284–287 (2012).
1217 115. Gu, Z., Gu, L., Eils, R., Schlesner, M. & Brors, B. circlize implements and
1218 enhances circular visualization in R. *Bioinformatics* **30**, 2811–2812 (2014).
1219 116. Pysam. pysam-developers (2023).
1220 117. Llorian, M. *et al.* Position-dependent alternative splicing activity revealed by
1221 global profiling of alternative splicing events regulated by PTB. *Nat. Struct. Mol. Biol.*
1222 **17**, 1114 (2010).

118. Conway, J. R., Lex, A. & Gehlenborg, N. UpSetR: an R package for the visualization of intersecting sets and their properties. *Bioinformatics* **33**, 2938–2940 (2017).
119. Siepel, A. *et al.* Evolutionarily conserved elements in vertebrate, insect, worm, and yeast genomes. *Genome Res.* **15**, 1034–1050 (2005).
120. Szklarczyk, Damian *et al.* STRING v11: protein–protein association networks with increased coverage, supporting functional discovery in genome-wide experimental datasets. *Nucleic Acids Res.* **47**, (2019).

Acknowledgments

S.W acknowledges financial support from the Emergent Algorithmic Intelligence Center of the Johannes Gutenberg University Mainz funded by the Carl-Zeiss-Stiftung. H.T. and S.G. acknowledge financial support from the Landesinitiative Rheinland-Pfalz and the Resilience, Adaptation, and Longevity (ReALity) initiative of the Johannes Gutenberg University of Mainz. J.W. acknowledges funding from the DFG (WI 3837/10-1).

Author information

Contributions

S.W. performed the bioinformatics analyses, interpreted and visualized the results. H.T. contributed to interpreting the results and performed statistical analyses. L.S. performed in-utero electroporation experiments and analyzed the data. L.Z. and S.M. performed immunostainings and analyzed the data. A.S. performed cell culture, RT-qPCR, and Western blot experiments. S.L.Z. performed Luciferase Assays. D.H. performed bioinformatics analyses. T.V. provided the *in vitro* neuronal differentiation model. DS and SS analyzed data and revised the manuscript. M.H. and S.G. provided supervision and organized funding. J.W. designed the research, supervised the study, and organized funding. S.W., H.T., and J.W. wrote the manuscript. All authors read and approved the final version of the manuscript.

Ethics declarations

Ethics approval

All animal experiments were performed in accordance with the regulations of the local authorities (Landesuntersuchungsamt Rheinland-Pfalz, license number 23 177-07/G 13-1-089).

Competing interests

The authors declare no conflict of interest.